An atlas of bacterial and viral associations in cancer

Sven Borchmann[1,2,3]

[1]University of Cologne, Department I of Internal Medicine, Center for Integrated Oncology Aachen Bonn Cologne Duesseldorf, German Hodgkin Study Group, Cologne, Germany

[2]University of Cologne, Faculty of Medicine and University Hospital of Cologne, Center for Molecular Medicine, Cologne, Germany

[3]University of Cologne, Faculty of Medicine and University Hospital of Cologne, Else Kröner Forschungskolleg Clonal Evolution in Cancer, Cologne, Germany

ABSTRACT

Bacterial[1,2] and viral[3–5] infections have widely been recognized as a cause of cancer. Examples for viral infections are Human Papillomaviridae causing cervical cancer[3,6,7] or Hepatitis B virus causing liver cancer[8,9]. An example for a bacterial infection is Helicobacter pylori causing adenocarcinoma of the stomach[10,11]. Known carcinogenic mechanisms are disruption of the host genome via genomic integration, expression of oncogenic viral proteins[12] or chronic inflammation[1].

Next generation sequencing has made it possible to gain deep insight into the cancer genome[13], while at the same time providing datasets with traces of bacterial and viral nucleic acids that colonize the examined tissue or are integrated into the host genome. This hidden resource has so far not been comprehensively studied.

Here, 3000 whole genome sequencing datasets are leveraged to gain insight into possible novel associations between viruses, bacteria and cancer. Apart from confirming known associations, multiple, previously unknown, possible associations between bacteria, viruses and tumors are identified. The presence of some bacteria or viruses was associated with profound differences in patient and tumor characteristics, such as patient age, tumor stage, survival, defined somatic alterations or gene expression profiles when compared to other patients with the same cancer.

Overall, these results provide a detailed map of potential associations between viruses, bacteria and cancer and can be the basis for future investigations aiming to confirm these associations experimentally and to provide further mechanistic insight.

INTRODUCTION

Bacterial[1,2] and viral[3–5] infections have widely been recognized as a cause of cancer with a wide range of carcinogenic mechanisms described. Examples for carcinogenic viruses are Human Papillomaviridae causing head and neck[14,15] as well as cervical cancer[3,6,7] or Hepatitis B virus causing liver cancer[8,9]. The main carcinogenic mechanisms at play are thought to be (1) viral integration into and disruption of the host genome and (2) expression of oncogenic viral proteins[12].

An important example for a carcinogenic species from the bacterial domain is Helicobacter pylori causing adenocarcinoma of the stomach[10,11]. The carcinogenic mechanism at play here is thought to be a totally different one compared to carcinogenic viruses, namely sustained inflammation caused by a chronic, mostly sub-clinical infection[1]. For some associations between infections and cancer, preliminary evidence has been presented but simultaneous presence of contradictory findings has led to widespread debate. An example for this is the finding that Fusobacterium nucleatum is enriched in cancerous tissue of colorectal cancer patients compared to tissue of benign adenomas or healthy colon mucosa[16–18]. Given the diversity of possible carcinogenic mechanisms[19] it is likely that other carcinogenic viruses and bacteria exist which are currently unknown.

Recent advances in next generation sequencing have made it possible to generate large amounts of data representing the whole genetic makeup of a tissue[13]. Resulting datasets contain traces of non-human, or, more general, non-host origin that is present either because of genomic integration or presence of the virus or bacteria in the tissue itself. While some studies have already been performed with the goal to repurpose this data to unravel novel

associations between infections and cancer[4,5,20–22], these resources have so far been underutilized to discover novel, possible associations between cancers and infections.

With this aim in mind, this study leverages a large, high-quality collection of over 3000 whole genome sequencing datasets to gain insight into possible novel associations between viruses, bacteria and cancer.

RESULTS

Samples

A total of 3,025 whole genome sequencing datasets comprising 3.79 trillion reads were included in this study (Figure 1A, Extended Data Table 1). These include 1,330 whole genome sequencing datasets of tumor tissue samples across 14 different cancers from 19 International Cancer Genome Consortium (ICGC)[23] studies and their corresponding matched normal (e.g. non-cancerous) tissue controls (n=1,330) (Extended Data Table 1). Included patients were predominantly male (n=1,028, 60.6%) and elderly, with 47.3% of patients (n=801) at least 60 years old (Figure 1B-C). Additionally, whole genome sequencing datasets from 365 subjects from the 1,000 genome project[24] were selected as a healthy control group substituting for the lack of negative sequencing controls to examine non-human DNA in the blood of healthy donors. Only subjects, in which blood-derived DNA was directly subjected to whole genome sequencing as opposed to DNA derived from immortalized lymphoblastoid cell lines (LCL) (subset analyzed, n=102) were included in the healthy control cohort as the whole genome sequencing datasets derived from LCL DNA showed a markedly different species-level taxon distribution likely representing taxa present due to LCL culture and not present in the donor itself (Extended Data Figure 2A, Supplementary Table 1, Supplementary Table 2). For validation purposes and to assess differential gene expression in cancers associated with certain species-level taxa all available matching RNA-Seq datasets for all included ICGC studies[23] were also analyzed (n=324).

Validation of Pipeline

Based on its high accuracy, especially with regard to precision and high speed necessary for handling large amounts of input data, a pipeline was built around KRAKEN[25], which at its core

is based on the exact alignments of k-mers to their least common ancestor (LCA). Before applying the pipeline to the datasets of interest, it was validated fourfold.

First, it was confirmed that the pipeline was able to identify already known bacterial and viral taxa in tissue-derived bacterial isolates and cell lines independent from this study. The pipeline was applied to a gastric mucosa isolate of Helicobacter pylori from a stomach ulcer patient (sample ID: SRS2800545, run ID: SRR6432709). As expected, 3,606,537/3,607,687 (99.97%) of read pairs matching any taxon in the database matched Helicobacter pylori (Supplementary Table 3, Extended Data Figure 2B). Next, the pipeline was applied to 3 cell line samples (HeLa (run ID: SRR1611000), CaSki (run ID: SRR1611128) and SiHa (run ID: SRR1611127)) with known integrations of Human papillomavirus[26]. Applying the pipeline resulted in between 78.14% and 99,90% of non-human read pairs matching any species-level taxon in the database to match Human papillomavirus 7 or 9 (Supplementary Table 3, Extended Data Figure 2B). Interestingly, the majority of non-human read pairs not matching Human papillomavirus 7 or 9 matched Mycoplasma hyorhinis (0.08%-21.74%), a common cell culture contaminant[27]. Thus, it was confirmed that the pipeline can identify bacterial and viral taxa irrespective of both a high level of human background DNA and whether the identifying sequence is present in the form of host-integrated DNA or by presence of the viral or bacterial taxa itself in the sample.

Second, it was confirmed that the taxonomic classification of non-human reads by the pipeline is highly correlated to the classification by an independent approach, namely mapping non-human reads to putative target genomes with BWA[28] (Supplementary Table 4, Extended Data Figure 2C-E).

Third, in yet another independent approach, it was confirmed that assembled contigs from non-human reads show high sequence similarity with the taxa identified by the pipeline (Supplementary Table 4, Extended Data Figure 2F).

Fourth, the pipeline was independently run with the same settings on available matched RNA-Seq and WGS data from the same tumor tissue samples. It was shown, that identified taxa in pairs of RNA-Seq and WGS data from the same tumor tissue sample are correlated both in a combined dataset of all pairs and for each sample separate for which RNA-Seq and WGS data was available (n=324) (Extended Data Figure 2 G-H). This validation is especially helpful to minimize the risk of contamination post sample processing though this was further mitigated with the data analysis strategy described below.

A map of cancer-associated taxa

Due to the nature of this dataset, which was not created with the purpose of analyzing the non-human taxonomic composition of cancer tissues, only a small fraction of sequence information can be used to infer taxa present in the respective sample. Therefore, less prevalent taxa are likely not detectable. Additionally, considering many samples will have been collected under sterile, surgical conditions, detected taxa are more likely to indicate true presence of that taxa in the tissue, limiting the detection of taxa that are part of the naturally occurring microbiome of non-sterile tissues, such as skin or bowel. Therefore, on average, only 2.2 species-level taxa per sample were detected, though variation was high (Supplementary Table 5, Extended Data Figure 3 A-D). For these reasons, many conventional methods of analysis of taxonomic composition are not applicable to this dataset and the focus of the present study is on identifying highly abundant species-level taxa that are potentially associated with cancer, either by being present in the patient's matched normal sample or

potentially more directly involved in carcinogenesis by being present in the patient's tumor tissue, especially when it is likely to have been collected sterile.

In this study, a total of 3,534,707 read pairs matching bacterial, viral or phage species-level taxa were detected across 19 studies in 3025 samples (Figure 1D-E, Extended Data Table 1, Supplementary Table 6). Subsampling of 10% of all read pairs did not alter the detected species-level taxa and their relative composition compared to analyzing all non-human read pairs which was validated in a subset of patients (Extended Data Figure 2I-J, Supplementary Table 7). A total of 218 species-level taxa could be identified in all examined samples (Figure 1F, Supplementary Table 8). Escherichia coli and Propionibacterium acnes were the most commonly detected species in all samples.

In order to control for differences in sequencing depth between samples, all raw read pair counts were normalized by dividing them by 1,000,000,000 total read pairs. This normalized count was defined as read pairs per billion (RPPB). Overall, 18,112 (+/- 4,238 standard error of mean (s.e.m.)), 20.003(+/- 4,295 s.e.m.) and 28,282 (+/- 9,081 s.e.m.) RPPB could be detected on average in healthy control samples from the 1000 genomes cohort, matched normal samples and tumor tissue samples, respectively, with a large variation across samples and sequencing projects (Figure 1G). Of note, particularly high RPPB were detected in matched normal, saliva-derived, samples from acute myeloid leukemia (AML) patients, as would be expected from a naturally non-sterile source such as saliva. The taxa with the highest RPPB are depicted in Figure 1H. Ralstonia pickettii was the species with the highest RPPB and almost absent in healthy donors, while being detected at higher levels in tumor tissue than in matched normal samples (Figure 1H). Except for Bacillus subtilis, Acidovorax sp. KKS102 and Bacillus cereus, all species with very high RPPB were detected predominantly in tumor tissue

or matched normal samples. A clustered heatmap of all species-level taxa detected in all samples is provided in Figure 2.

Next, filtering was performed to exclude taxa that were (i) frequently detected in the healthy control group, (ii) detected only in very few (<5) tumor tissue or matched normal samples, (iii) detected phages, (iv) taxa that are commonly detected as part of the normal oral microbiome and were mainly detected in saliva, oral or esophageal cancer tissue samples (Supplementary Table 9), (v) taxa that have been previously described as sequencing contaminants (Supplementary Table 10) and (vi) taxa, for which the detected reads were unevenly distributed across their genome (Extended Data Figure 4). After all these filtering steps (Extended Data Figure 5) 27 species-level taxa remained for further analysis (Figure 1 I-J, Extended Data Figure 6, Supplementary Table 8).

Among these, known tumor-associated taxa, such as Hepatitis B virus[8,9] or Salmonella enterica[29,30] were detected. Additionally, taxa were detected that have been implicated in carcinogenesis before without enough evidence to support a carcinogenic role, such as Pseudomonas species[31,32] and taxa that have never been implicated in carcinogenesis before, such as Gordonia polyisoprenivorans. Of note, most taxa in the final filtered species list were detected at much higher RPPB-levels in tumor tissue compared to matched normal samples, though most matched normal tissues in this study were blood-derived. However lower RPPB could still be detected in matched normal samples and across all taxa tumor tissue samples and matched normal samples are highly correlated (Extended Data figure 2K).

In order to better understand the association of detected taxa with different cancers and among each other, a heuristic approach was used combining the non-linear dimensionality reduction and visualization method t-distributed stochastic neighborhood embedding (t-SNE)

with K-means clustering. To focus on taxa that potentially play a more direct role in carcinogenesis and considering that RPPB of detected taxa were highly correlated between tumor tissue and matched normal tissue with lower levels detected in matched normal tissue (Extended Data Figure 2K), only tumor tissues were included in the following analyses.

Using a pan-cancer approach, a combined dataset of all tumor tissue samples was visualized using t-SNE using the $\log_2$-transformed RPPBs of all detected non-phage taxa (n=204) as input variables. First, two distinct groups of patients with chronic lymphocytic leukemia (CLL) emerged. One group (n=24) was associated with presence of Gordonia polyisoprenivorans in the patient's tumor tissue and another group (n=15) was associated with tumor tissue presence of Pseudomonas mendocina. Second, one distinct group (n=23) of pancreatic cancer patients associated with presence of Cupriavidus metallidurans was observed. Third, one group (n=22) of bone cancer patients associated with presence of Pseudomonas poae, Pseudomonas fluorescens and Pseudomonas sp. TKP could be distinguished. Fourth, a group of patients (n=14) with bone cancer (n=4) and chronic myeloid disorders (n=10) associated only with presence of Pseudomonas sp. TKP was observable (Figure 3A). Overall, this approach was helpful to get a first insight into groups of tumors from a pan-cancer perspective that might be defined by presence or absence of specific taxa.

In order to gain further insight into the association of detected taxa and specific cancers, each cancer (Supplementary Table 11) was examined separately, visualizing patient groupings using t-SNE with $\log_2$-transformed RPPBs of all the final filtered taxon list (n=27) (Supplementary Table 1) in tumor tissue as input variables combined with K-means clustering of patients using the same input variables. Additionally, each cluster was associated with age, survival, gender, number of alterations in known cancer genes or specific alterations in one of those cancer genes.

For bone cancer patients this dual methodology revealed a cluster of patients with presence of Pseudomonas fluorescens, Pseudomonas sp. TKP and Pseudomonas poae (cluster 2) in the tumor tissue, confirming the results of the pan-cancer approach used above (Figure 3B, Extended Data Figure 7A).

For chronic lymphocytic leukemia patients this approach revealed 3 clusters, one of patients with presence of Gordonia polyisoprenivorans in the tumor tissue (cluster 3), one of patients associated with Human Mastadenovirus C (cluster 2) and one with the remainder of patients (cluster 1), some of which showed presence of Pseudomonas species in the tumor tissue. Clusters could be identified by both methods, t-SNE and K-means (Figure 3C, Extended Data Figure 3B). The clusters representing patients associated with Gordonia polyisoprenivorans (cluster 3) and Human Mastadenovirus C (cluster 2) were mutually exclusive ($p_{Fisher} = 0.0124$) (Figure 3C, Extended Data Figure 7B). There was a tendency towards different ages at diagnosis between the clusters ($p_{anova}=0.0743$) (Figure 4A). Additionally, there was a tendency towards a difference in survival between the different clusters ($p_{anova}=0.0745$). Patients in cluster 1 (no associations) had worse survival than patients in cluster 2 (Human Mastadenovirus C) or 3 (Gordonia polyisoprenivorans) ($p=0.024626$) (Figure 4B). Patients with an association with Gordonia polyisoprenivorans (cluster 3) were more likely to be of Binet C stage (5/36 vs. 1/61, C vs. not-C, $p_{Fischer} = 0.0252$) (Figure 4C). These patients were also more likely to be associated with TP53 mutations than patients in the other clusters (p_{Fisher}(cluster 3 vs. other)=0.0335) (Figure 4D).

For esophageal cancer patients 3 clusters were identified. K-means clustering revealed one cluster of patients with presence of Human Herpesvirus 5 (cluster 3) in the tumor tissue and one cluster with presence of Bifidobacterium dentium (cluster 2). The remaining cluster contained patients with no discernable associations. However, these 3 clusters could not be

differentiated by t-SNE. (Figure 3D, Extended Data Figure 7C). There was a tendency towards different numbers of alterations in cancer genes between clusters (p_{anova}=0.0858), with patients in cluster 3 (Human Herpesvirus 5) having less alterations than patients in cluster 1 (no associations) and 2 (Bifidobacterium dentium) (p=0.0392) (Figure 4E). Additionally, there was a tendency towards a difference in survival between the different clusters (p_{anova}=0.1). Patients in cluster 2 (Bifidobacterium dentium) or 3 (Human Herpesvirus 5) had worse survival than patients in cluster 1 (no associations) (p=0.040928). (Figure 4F).

Patients with liver cancer could be grouped into 4 clusters with K-means clustering and t-SNE agreeing. One cluster was defined by presence of Hepatitis B (cluster 1) in the tumor tissue. A second cluster was defined by sole presence of both Pseudomonas and Serratia species (cluster 3). A third cluster was defined by additional presence of Parvibaculum lavamentivorans and Human Herpesvirus 5 as well as two additional Pseudomonas species, Pseudomonas poae and Pseudomonas protegens (cluster 4), in addition to those detected in the previous cluster. The fourth cluster contained patients with no discernable associations (cluster 2) (Figure 3E, Extended Data Figure 7D). There was a tendency towards different ages at diagnosis between the clusters (p_{anova}=0.0015) with patients in cluster 1 (Hepatitis B), cluster 2 (Pseudomonas and Serratia sp.) and cluster 4 (Pseudomonas sp., Serratia sp. Parvibaculum lavamentivorans and Human Herpesvirus 5) younger than patients in cluster 3 (no associations) ($p_{t\text{-}test}$=0.000142) (Figure 4G). In a similar pattern, these patients had had a higher frequency of alterations in RNF21 ($p_{Fischer}$ = 0.0121) (Figure 4H).

For patients with pancreatic adenocarcinoma 5 clusters could be identified using K-means clustering. The first cluster was defined by presence of Pseudomonas protegens in the tumor tissue (cluster 5), the second by Methylobacterium populi (cluster 4) and a third, prominent cluster was defined by presence of Cupriavidus metallidurans (cluster 2). The two other

clusters contained patients with no discernable associations (cluster 1 and 3). Only the cluster of patients associated with Cupriavidus metallidurans (cluster 2) could also be identified using t-SNE (Figure 3F, Extended Data Figure 7E). Differences in the frequency of alterations between patients in different clusters were observed in KMT2C, CDKN2A and RNF21. Patients in cluster 2 (Cupriavidus metallidurans) ,4 (Methylobacterium populi) or 5 (Pseudomonas protegens) had a higher frequency of alterations in these genes compared to the majority of patients which were in cluster 1 (no associations) (n=187) (p_{Fisher}(KMT2C)=0.0308, p_{Fisher}(CDKN2A)=0.0124, p_{Fisher}(RNF21)=0.0107) (Figure 4I-K).

For patients with prostate cancer, 5 clusters emerged using K-means clustering, one defined by simultaneous presence of Thauera sp. MZ1T, Cupriavidus metallidurans and Pseudomonas mendocina in the tumor tissue (cluster 5), one by presence of Pseudomonas sp. TKP (cluster 3) and another one by presence of Gluconobacter oxydans and Rhodopseudomonas palustris (cluster 2). The two other clusters contained patients with no discernable associations. Out of these, the cluster defined by Gluconobacter oxydans and Rhodopseudomonas palustris (cluster 2) and the one defined by Thauera sp. MZ1T, Cupriavidus metallidurans and Pseudomonas mendocina (cluster 5) could be confirmed using t-SNE (Figure 3G, Extended Data Figure 7F). There were age differences at diagnosis observable between the clusters (p_{anova}=0.00994) with patients in cluster 2 (Gluconobacter oxydans) and 5 (Rhodopseudomonas palustris) older than the other patients ($p_{t\text{-}test}$)=0.000544) (Figure 4M).

For patients with renal cancer a cluster of patients associated with Serratia marcescens (cluster 2) was identified using K-means clustering, although t-SNE did not separate this group of patients (Figure 3H, Extended Data Figure 4N). The other cluster contained patients with no discernable associations (cluster 1). There was a tendency towards a higher frequency of PBRM1 alterations in patients in cluster 1 (p_{Fisher}=0.0723) (Figure 4P).

For patients with pancreatic endocrine neoplasms, ovarian cancer, chronic myeloid disorders and breast cancer, no discernable clusters emerged (Extended Data figure 8A-D).

Unbiased association analysis between taxa and patient features

In addition to associating the above identified clusters with patient features, an unbiased analysis of possible associations between presence of a species-level taxa and patient features, such as age, survival, gender, number of alterations in known cancer genes and specific alterations in one of those cancer genes was performed in both a pan-cancer approach using the whole dataset and analyzing each cancer separately. In this exploratory analysis, all non-phage taxa detected (n=204) were included and multiple testing correction was performed.

Association between taxa and patient age

In the pan-cancer analysis, no association remained significant at the α=0.05 level after correction for multiple testing. However, looking at each cancer separately, several associations were identified. A group of bacterial taxa was associated with older patients in prostate cancer (Figure 4L). In chronic myeloid dysplasia, presence of Pseudomonas sp. TKP was associated with older age (p_{adj}=0.039) (Figure 4Q).

Association between taxa and patient survival

In the pan-cancer analysis, no association remained significant at the α=0.05 level after correction for multiple testing. However, looking at each cancer separately, presence of several taxa had a significant impact on survival at the α=0.05 level. In renal cancer, presence of Ralstonia pickettii was associated with improved survival, in fact no patient died (p_{adj}=0.035) (Figure 4O).

Association between taxa and patient gender

For both the pan-cancer analysis and looking at each cancer separately, no significant associations were found at the α=0.05 level after correcting for multiple testing.

Association between taxa and number of genetic alterations in cancer genes

In the pan-cancer analysis, no association remained significant at the α=0.05 level after correction for multiple testing. However, looking at each cancer separately, presence and higher RPPB matching P. acne was associated with a decreasing number of alterations in prostate cancer (p_{adj}=0.0041) (Figure 4N).

Association between taxa and specific genetic alterations

For both the pan-cancer analysis and looking at each cancer separately, no significant associations were found at the α=0.05 level after correcting for multiple testing.

Somatic lateral gene transfer

The integration of viral nucleic acids into the human host genome is well recognized as a carcinogenic process. High-level evidence exists for the integration of Hepatitis B[8,9], Human Papillomavirus[6,7] and Epstein–Barr virus (Human Herpesvirus 4)[33,34], which are causally linked to hepatocellular carcinoma, cervical cancer and lymphoma, respectively. Additionally, some evidence for somatic lateral gene transfer from bacteria to cancerous tissue has been presented before[20] and subsequently controversially discussed.

Aiming to find evidence for bacterial or viral DNA integrated into the human host genome in this dataset, a pipeline was developed to do so. In brief, read pairs in which one read mapped to the human genome and one read to one of the taxa in the final filtered taxon list (n=27)

were counted and then compared to the number of read pairs in which both reads mapped to the respective taxa. The number of divergently mapping read pairs divided by the number of complete pairs mapping that respective taxa was used as an indicator for potential genomic integration and lateral gene transfer. This was done separately for the tumor tissue datasets and the matched normal datasets for all patients for which the pipeline revealed at least 1000 RPPB matching one of the taxa in the final filtered taxon list (n=27) in that respective patient's tumor tissue sample (n=79, Supplementary Table 2). The resulting data is shown in Supplementary Table 1 and Extended Data Figure 4. The highest rate of integration was observed for Hepatitis B in tumor tissue (9.62%) (Extended Data Figure 9A). Across all analyzed taxa, putative integrations were more common in matched normal samples than in tumor tissue samples (p=0.0009, Wilcoxon paired signed rank test) (Extended Data Figure 9B) and for viral taxa compared to bacterial taxa (p=0.0001, Mann-Whitney U-test) (Extended Data Figure 9C). In conclusion, there was no evidence for a general phenomenon of lateral gene transfer for the final filtered taxon list, with the exception of Hepatitis B, for which integration into the cancer genome has been widely described[8,9].

Results of differential gene expression analysis

Differential gene expression analysis was performed for all taxa and cancer combinations with available RNA-seq data and in which at least 5 patients had at least 100 RPPB matching the respective taxon (Supplementary table 10). Differentially expressed genes (q<0.05) were identified for chronic lymphocytic leukemia patients with or without detection of Gordonia polyisoprenivorans (258 genes) (Figure 5A, Supplementary table 12), Human Mastadenovirus C (1725 genes) (Figure 5B, Supplementary table 13) and Pseudomonas aeruginosa (50 genes, Supplementary table 14). Furthermore, differentially expressed genes were identified for ovarian cancer patients with or without detection of Escherichia coli (22 genes)

(Supplementary table 15) and pancreatic adenocarcinoma patients with or without detection of Propionibacterium acnes (3 genes) (Supplementary table 16). Next, differential gene expression data was used to perform bidirectional functional enrichment in order to identify pathways that are altered in patients with or without presence of the respective taxon. To no surprise, only the two associations with a significant number of differentially expressed genes, chronic lymphocytic leukemia with or without presence of Gordonia polyisoprenivorans (Supplementary table 17) or Human Mastadenovirus C (Supplementary table 18), respectively, showed enrichment in some pathways.

Overall, presence of Gordonia polyisoprenivorans lead to a gene expression pattern indicative of a decreased level of mitotic cell cycling. Also, a gene expression pattern indicative of a decreased DNA damage response was observed. Additionally, a gene expression pattern indicative of reduced blood coagulation and reduced macrophage activation was observed in patient samples with presence of Gordonia polyisoprenivorans (Figure 5C).

Contrary to that, presence of Human Mastadenovirus C lead to a gene expression pattern that is indicative of an increase in B-cell proliferation and a reduction of various immune defense functions, such as immune response in general, Tumor necrosis factor and interleukin beta 1 production, activated T cell proliferation and a decrease in cytokine secretion in general. In addition, the altered gene expression pattern of patients with presence of Human Mastadenovirus C is indicative of a markedly reduced DNA damage response (Figure 5D).

DISCUSSION

The aim of this this study was to leverage a large, high-quality dataset of over 3000 samples to unravel novel associations between viral and bacterial taxa and cancer. A total of 218 species-level taxa could be identified in tumor tissue, matched normal and healthy donor samples. Out of these, 27 taxa remained being likely cancer-associated after extensive filtering. While studies on the viral metagenome of caner tissues and patients have been performed using datasets from cancer genomics studies[4,5,21,22], similar large studies looking at the bacterial metagenome are lacking.

Studies examining the viral metagenome of cancer tissues mainly identified known associations of Human Papillomavirus with cervical and head and neck cancer, Hepatitis B in liver cancer and Human Herpesvirus 5 in a variety of cancers while detection of Human Mastadenovirus C was controversial[4,5,21,22].

Smaller studies examining bacteria-tumor associations in pan-cancer datasets have identified Escherichia coli, Propionibacterium acne and Ralstonia pickettii in multiple cancers, while more specifically finding Acinetobacter sp. in AML and Pseudomonas sp. in both AML and adenocarcinoma of the stomach[20,35]. Interrogating cancer-specific datasets, Salmonella enterica, Ralstonia pickettii, Escherichia coli and Pseudomonas sp. were detected in breast cancer and adjacent tissue[36], while Escherichia sp., Propionibacterium sp., Acinetobacter sp. and Pseudomonas sp. were frequently detected in prostate cancer[32]. Confirming the findings of the present study, these smaller studies found similar bacterial taxa, especially Ralstonia pickettii, Escherichia coli, Propionibacterium acne Salmonella enterica and Pseudomonas sp. Interestingly, the present study identified a number of taxa that have not been previously identified in cancer tissue or matched normal samples of these patients, among them

Cupriavidus metallidurans, Gordonia polyisoprenivorans, Serratia sp. and Bifidobacterium sp.. Reasons for this are likely the much higher (1) number and diversity of patients and samples included, (2) the larger amounts of data examined per sample due to having higher-coverage WGS datasets available for all patients compared to RNA-seq or whole-exome sequencing (WXS) datasets in previous studies and (3) the optimized and extensively validated bioinformatics approach used herein. Of note, the filtering strategy used in this study to exclude taxa likely resulting from contamination has also eliminated bacterial taxa that have been linked to cancer previously such as Escherichia coli and Propionibacterium acne, mainly due to the frequent detection of these taxa in healthy donor samples from the 1000 genome cohort. Stringent filtering for species-level taxa that have been detected at 2 $\log_{10}$-levels higher in tumor tissue or matched normal tissue compared to healthy donor samples excluded these species, despite having about 1.4x and 3.1x higher RPPB for matched normal and tumor tissue, respectively, compared to healthy donors for Propionibacterium acne. These values were even higher for in the case of Escherichia coli, namely 7.1x and 13.4x for matched normal and tumor tissue, respectively. Thus, it cannot be excluded that tumor-associated taxa were eliminated due to the stringent filtering utilized.

Looking at specific cancer-pathogen associations, a subgroup of bone cancer patients with presence of Pseudomonas sp. in the tumor tissue was identified. Consistent associations between viral or bacterial taxa and bone cancer have not been described before, apart from some evidence linking simian virus 40 (SV40) infection to bone cancer[37]. Interestingly, Pseudomonas sp. are frequently implied in difficult to treat cases of osteomyelitis. Thus, one might speculate that chronic, subclinical infection exists and could be carcinogenic.

For CLL patients, two associations were identified, one with Gordonia polyisoprenivorans and one with Human Mastadenovirus C. Gordonia polyisoprenivorans has not been implied in

cancer before. Interestingly, the bacterium has been identified as a rare cause of bacteremia, so far exclusively in patients with hematological cancers[38–40]. While the immunosuppression associated with hematological cancers and subsequent treatment obviously predisposes to infections with unusual pathogens from the environment, it is at least possible that these patients had a latent infection with Gordonia polyisoprenivorans which exacerbated into bacteremia and sepsis upon treatment-induced immunosuppression. Human Mastadenovirus C has to date not been clearly linked to cancer, though two recent reports have found it frequently in various cancer tissue, with one treating it as contamination[4] and one not[21] (see methods for a detailed discussion). Further indirect evidence for a possible role of both Gordonia polyisoprenivorans and Human Mastadenovirus C in CLL carcinogenesis is provided by (1) the observed age difference - patients with detection of Human Mastadenovirus C were markedly younger, (2) the mutual exclusivity of detection of Gordonia polyisoprenivorans and Human Mastadenovirus C and (3) the fact that survival was different - patients with detection of either taxa had improved outcome. This was despite patients associated with Gordonia polyisoprenivorans having a higher likelihood of having Binet C stage. Providing a possible explanation for the observed survival benefit, patients with no taxa association (cluster 3) had a higher likelihood of having TP53 mutations. Strikingly, marked differences in host gene expression between patients in which one of the taxa was detected and other patients were observed. The observed gene expression pattern for patients associated with Gordonia polyisoprenivorans, especially an increased DNA damage response and reduced mitotic cell cycling, could explain the improved survival of these patients. The gene expression pattern observed for patients associated with Human Mastadenovirus C pointed towards reduced immune activity, especially reduced T cell function and a decrease in cytokine production and secretion, which could explain the observed high detection frequency of Human

Mastadenovirus C DNA in line with an uncontrolled infection due to a diminished immune response. Detection of Mastadenovirus C was associated with a decreased DNA damage response, which has been described as being an important pathomechanism of CLL[41]. In addition to CLL patients, both Gordonia polyisoprenivorans and Human Mastadenovirus C were also detected frequently in other cancers, sometimes at high levels, while never being detected in healthy donors.

Two taxon-tumor associations in esophageal cancer were identified, one with Bifidobacterium dentium and one with Human Herpesvirus 5. Interestingly, patients in cluster 3 (Human Herpesvirus 5) had less alterations in cancer gene consensus genes than the other patients, pointing to a possible different carcinogenic mechanism, where the accumulation of multiple somatic alterations is not stringently needed for malignant transformation. Furthermore, patients in cluster 1 (without any association with Bifidobacterium dentium or Human herpesvirus 5) had better survival. While the association of Human Herpesvirus 5 with esophageal cancer is a novel finding, Human Herpesvirus 5 has frequently be detected in adjacent adenocarcinoma of the stomach[5]. Of note, overt Human Herpesvirus 5 esophagitis can occur in immunocompromised hosts[42], which could be indicative of a latent infection of the esophagus by Human Herpesvirus 5 in some hosts.

In patients with liver cancer, one subgroup of patients was defined by detection of Hepatitis B, a known cause of liver cancer[8,9]. Interestingly, two other subgroups could be identified. Pseudomonas sp. and Serratia sp. were detected in both groups, with additional detection of Parvibaculum lavamentivorans and Human Herpesvirus 5 in one group. There are some hints that Human Herpesvirus 5 might play a role in the carcinogenesis of liver cancer, among them presence of CMV DNA in tumor tissue and an increased seroprevalence in liver cancer patients[43] as well as frequent hepatitis in Human Herpesvirus 5 infection underscoring

hepatotropism of Human Herpesvirus 5[44]. The other identified taxa have not yet been implied in liver cancer carcinogenesis. Compared to patients not associated with one of the taxa identified in liver cancer tumor tissue samples, all patients with presence of any identified taxa were younger. Hepatocellular carcinoma at younger age is associated with chronic Hepatitis B infection[45]. Since younger age was also observed in patients associated with the other taxa, one might speculate that liver cancers associated with other pathogens are associated with younger age of onset as well.

Three bacteria-tumor associations were identified in pancreatic adenocarcinoma, one with Pseudomonas protegens, one with Methylobacterium populi and one with Cupriavidus metallidurans. While Pseudomonas sp. have been shown to be a contributor to the pancreatic adenocarcinoma tissue microbiome[31], Methylobacterium populi and Cupriavidus metallidurans have not been detected in cancer tissue. In fact, both taxa have not been discovered in human hosts but in environmental samples and are thus not considered to be part of the human microbiome, making it possible that they are contaminants not truly present in the tumor tissue samples analyzed. On the other hand, few infections of humans by these taxa have been described[46,47] and, of note, the first published report of a Cupriavidus metallidurans infection was a case of septicemia in a patient with a pancreatic tumor[47].

In patients with prostate cancer, the most interesting findings were age differences between patient clusters defined by the presence of different taxa and a negative correlation of Propionibacterium acne presence and number of alterations in cancer gene consensus genes. Patients in cluster 2 (defined by Gluconobacter oxydans and Rhodopseudomonas palustris) and cluster 5 (defined by Thauera sp. MZ1T, Cupriavidus metallidurans and Pseudomonas mendocina) were markedly older than the other patients. Gluconobacter sp., Rhodopseudomonas sp., Cupriavidus sp. and Pseudomonas sp. have previously been

identified in prostate cancer and normal prostate tissue[32], but their precise role in prostate disease is entirely unclear. Propionibacterium acne has been implied as a potential carcinogenic bacterium in prostate cancer[48,49], possibly by creating a chronic inflammatory microenvironment[50]. Like Human Herpesvirus 5 in esophageal cancer, the reduced number of alterations in cancer gene consensus genes upon increased Propionibacterium acne frequency could point to alternative carcinogenesis by chronic inflammation in the absence of the accumulation of many mutations in putative cancer driver genes.

For patients with renal cancer, an association with Serratia marcescens was described for a subgroup of patients. While Serratia marcescens has been described as a frequent cause of urinary tract infections, especially in immunocompromised hosts in a nosocomial setting[51], it has so far not been implicated in cancer. Interestingly, survival of patients with detection of Ralstonia pickettii in their tumor tissue was markedly improved. Ralstonia pickettii is a bacterium that has been filtered out in this study because of frequent detection in healthy donor samples. It could be speculated, that, while not causing any overt infection, low level presence of Ralstonia pickettii in the human host is common, and improves immunogenicity of renal cancer and, thus, improving outcome. It has been shown, that alterations of local and systemic immunity by a host's microbiome possibly influence the anticancer immune response[52], which might be highly relevant for a naturally immunogenic tumor, such as renal cancer[53].

The intriguing observation of increased somatic bacteria-human lateral gene transfer by Riley et al. [20] could not be made in this study. The only taxa for which more integration into the host genome was observed in tumor tissue compared to matched normal was Hepatitis B, for which integration into the genome of cancerous cells has been well recognized[54].

In conclusion, the present study provides an important, unprecedented atlas of potential associations between both bacterial and viral taxa with cancer. In addition to confirming known or postulated associations between cancers and viral or bacterial taxa, several novel associations were identified for the first time, laying the groundwork for experimental validation and further mechanistic studies.

METHODS

Data sources

Mapped sequencing data for the included ICGC studies was obtained via the ICGC DCC[23,55] and downloaded using customized scripts. The use of controlled access ICGC data for this project was approved by the ICGC Data access compliance office. Mapped sequencing data for the 1000 genome healthy control samples was obtained from the 1000 genome FTP server[56] using customized scripts. Sequencing data used for validation was obtained from the European Nucleotide Archive (ENA)[57].

Computing environment

Data analysis was performed using a HP Z4 workstation in a Unix environment either using standalone standard tools as mentioned throughout the methods section or customized scripts. Some analyses were performed employing the Galaxy platform[58].

Pipeline for taxonomic classification

First, unmapped (non-human) read pairs were extracted from downloaded sequencing data using Samtools (version 1.7)[59]. Bam files were sorted by query name with Picard Tools (version 2.7.1.1)[60] and converted to FastQ files using Bedtools (version 2.26.0.0)[61]. Subsequently, Trimmomatic (version 0.36.3)[62] was used to trim reads with sliding window trimming with an average base quality of 20 across 4 bases as cutoff and dropping resulting reads with a residual length < 50. Read pairs, in which one read was dropped according to these rules were dropped altogether. Remaining read pairs were joined with FASTQ joiner (version 2.0.1)[63] and converted to FASTA files using the build-in function FASTQ to FASTA (version 1.0.0) from Galaxy[58]. Next, VSearch (version 1.9.7.0)[64] was used to mask repetitive sequences by replacing them with Ns using standard settings. These masked and joined read pairs were fed into

Kraken (version 1.2.3)[25] using a database of all bacterial and viral genomes in Refseq. The output of each run was filtered with Kraken (version 1.2.3)[25] setting a confidence threshold of 0.5. A report combining the output of all samples and runs was generated using Kraken (version 1.2.3)[25]. The output was then arranged using customized scripts in R (beginning with version R 3.3.2. and subsequently updated)[65] to generate the raw metagenome output of each sample. Next, the raw outputs of each sample running the pipeline on a subset of 10% of the cancer tissue and matched normal sample read pairs and on all non-human read pairs of the 1000 genomes samples were filtered by only including species-level taxa and excluding all species-level taxa that were supported by less than 10 read pairs across all samples using R (beginning with version R 3.3.2. and subsequently updated)[65]. Read pairs assigned to Enterobacteria phage phiX174 which is ubiquitously used as a spike-in control in next generation sequencing were omitted from all counts as an intended contaminant.

To correct for the variation of sequencing depth across samples, matched read pairs per billion read pairs raw sequence (RPPB) were calculated for each sample and each taxon. A taxon was heuristically considered detected, when a respective sample had at least 100 RPPB assigned to that taxon.

Filtering strategy

First, all taxa that were also highly prevalent in the healthy control group, were excluded from further analysis. In detail, a taxon had to have an at least 2 $\log_{10}$-levels higher mean RPPB across either the tumor tissue samples, or the matched normal samples compared to the healthy control samples. This cutoff excluded all taxa that were also highly prevalent in the healthy control samples while at the same time allowing to further analyze taxa that were enriched in matched normal samples such as blood as well as taxa that were dominant in

tumor tissue. After this step, 147/218 (67.4%) potential tumor-associated species-level taxa remained. Next, taxa that were detected in fewer than 5 tumor tissue or matched normal samples were excluded (n=78), as well as all remaining phages (n=2). Hepatitis B as a known cancer-associated virus was re-included despite being present in fewer than 5 tumor tissue or matched normal samples so that 68/218 (31.2%) taxa remained.

Taxa that survived this filtering strategy were likely to be tumor-associated but could also represent artifacts from contamination. To account for that, all taxa were filtered out that are known to be regularly present in the oral microbiome[66–68] and were at the same time mainly (>50% of all RPPB matching a respective taxon) detected in samples that are likely contaminated with the oral microbiome (saliva matched normal, oral cancer tissue and esophageal cancer tissue samples) (Supplementary Table 9). Exemplary, this filtered out taxa that are a commonly present in the oral human flora such as Streptococcus mitis and were indeed mainly present in tumor tissue samples of oral cancer or esophageal cancer and likely a contaminant based on the biopsy location or detected in the matched normal of leukemia cases whose matched normal was a saliva sample likely containing taxa of the normal human microbiome. After this filtering step 49/218 (22.5%) species-level taxa remained.

It has recently emerged that both reagents and kits used in DNA extraction and library preparation as well as ultrapure water used in laboratories can contain contaminants that can hamper the detection of truly present taxa in low biomass or high background (e.g. human) samples. As this study was performed using samples that were both, low in non-human biomass and in the context of high human background the aim was to further reduce false positives by compiling a list of common contaminants in microbiome studies from the literature. Recommended approaches, such as the sequencing of blank controls[69] were not feasible as the present study was conducted utilizing already sequenced primary material.

Therefore, a database of common contaminants from various studies[70–74] examining this issue was compiled (Supplementary Table 10). All previously recognized contaminant taxa apart from those that were described as a contaminant on genus-level but where different species within the genus were associated differently with 1000 genome control samples and matched normal or tumor tissue samples were excluded. This was the case for the genera Pseudomonas and Methylobacterium. While the species Pseudomonas aeruginosa, Pseudomonas putida and Pseudomonas stutzeri were associated with both 1000 genome control and matched normal or tumor tissue samples and thus likely contaminants, Pseudomonas fluorescens, Pseudomonas mendocina, Pseudomonas poae, Pseudomonas protegens and Pseudomonas sp. TKP were not present in 1000 genome healthy control samples. Thus, it is likely, that the species-level resolution of this analysis was able to differentiate between common contaminants and possibly tumor-associated taxa. Similarly, differentiation was possible between Methylobacterium radiotolerans and Methylobacterium extorquens (likely contaminants) and Methylobacterium populi, which was only found in tumor-associated samples. The same held true for Cupriavidus metallidurans and Propionibacterium propionicum. After this filtering step, 27/218 (12.4%) species-level taxa remained (Figure 1 I-J, Extended Data Figure 6). While it cannot be ruled out that all these filtering steps removed cancer-associated taxa, the aim was to be cautious and rather accept a false-negative than a false-positive finding. Of course, experimental validation of the relevance of one of the taxa eliminated by one of the filters could prove that this taxon is both, a sequencing contaminant and a relevant taxon in cancer.

If a taxon is indeed present in a tissue, matching read pairs are expected to be uniformly distributed across its genome. Consequently, a further filtering step examining this was introduced. The sequencing data from all samples was combined and matched against a

reference database constructed out of the genome of these 27 taxa. Next, the coverage distribution of reads across each genome was assessed (Extended Data Figure 4). If the respective taxa are indeed present in the sample and not the result from misalignment or sequence similarity of certain parts of the genome an uneven coverage would result. It was found that all read pairs matching Human Mastadenovirus C aligned to short parts of its genome with a maximum length of a few hundred base pairs and abrupt drops in coverage (Extended Data Figure 4). This was also found in another study using different cancer tissue sequencing data and resulted in excluding Mastadenovirus C from further analysis[4]. Using Blast (beginning with version 2.7.1 and subsequently updated)[75] it was found that read pairs matching Human Mastadenovirus C aligned all equally well to commonly used cloning vectors, such as pAxCALGL which might have been used in the production of reagents used for sequencing. This form of contamination was recently analyzed and found to be frequent[76]. However, read pairs aligning to Human Mastadenovirus C originated from very few, seemingly unlinked samples from diverse cancer sequencing projects, making contamination by recombinant DNA unlikely. Another possible explanation for the observed coverage pattern is somatic genomic integration of parts of the Human Mastadenovirus C genome into a specific cancer genome. A recent analysis of PCAWG data focusing on viruses in cancer with overlap to patients and samples analyzed within this study also identified presence of Human Mastadenovirus C in cancer tissue and included it in their analysis among other viruses[21]. On balance, Human Mastadenovirus C was therefore not excluded from further analysis as an at least possible cancer associated viral taxon.

Clustering of pipeline hits

T-SNE was performed using a web-based TensorFlow Embedding Projector implementation[77]. The learning rate and the perplexity were heuristically set to 10 and 30 for all analyses,

respectively, except for the liver cancer subset, for which the perplexity was set to 50 due to improved cluster discrimination. The number of iterations was heuristically chosen, so that no major changes of cluster composition occurred upon increasing the number of iterations. Depending on the subset analysis, between 500 and 1500 iterations were needed to reach that point. T-SNE was performed in 3 dimensions for the pan-cancer analysis and in 2 dimensions for the cancer-specific analyses.

K-means clustering was performed using Morpheus[78]. Unsupervised K-means clustering using Euclidean distance as a similarity measure was employed with the number of clusters being heuristically informed by combining visual inspection, comparing t-SNE and K-means clusters and by examining marginal reduction of within-group variance with increasing numbers of clusters (i.e. the elbow method) (Extended Data Figure 10 A-J).

To combine the information obtained by both complimentary methods, t-SNE clustering was repeated with the same settings for each analysis, while color-coding clusters inferred from K-means clustering.

Assessment of taxonomic differences between cell culture-derived DNA samples and blood-derived DNA samples from the 1000 genome project

All taxa in the final taxon list (n=218) (Supplementary Table 19) which were identified in blood-derived 1000 genomes healthy control samples were selected (n=76) (Supplementary Table 11). The pipeline was subsequently applied to randomly selected (identifier ending with 8 or 9) LCL-derived 1000 genomes samples (n=102) (Supplementary Table 12). Finally, RPPB in these LCL-derived samples were calculated for all 76 taxa that were identified in the blood-derived 1000 genomes samples and compared between blood-derived and LCL-derived samples.

Proof that subsampling of read pairs does not alter relative taxon distribution

To show that subsampling does both not alter the detected species-level taxa and their relative composition compared to analyzing all non-human read pairs, a subset of 184 tumor tissue samples (Supplementary Table 15) was analyzed completely without any subsampling and subjected to the pipeline in the same way as in the main analysis. Exemplary, read pairs matching Human Mastadenovirus C, P. poae, R. pickettii and P. acnes were used to compare absolute read pair counts between full data and the subsample for all taxon-sample pairs in which the 10% subsample had at least 10 matches to the respective taxon.

Pipeline validation strategy

In order to perform in-depth validation of the pipeline, two alternative strategies were compared to the results obtained from it.

In the first alternative strategy, BWA mem (version 0.7.17) [79] was used to align read pairs to downloaded representative bacterial and viral genomes for the final filtered taxon list (Supplementary Table 1, Accession numbers in Supplementary Table 16). In detail, Samtools (version 1.7)[59] was used to merge all non-human mapped BAM files. Next, read pairs were extracted using Samtools (version 1.7)[59] and mapped to phiX (Coliphage phi-X174, complete genome, NC_001422.1) with BWA mem (version 0.7.17)[79]. Using Samtools (version 1.7)[59] all read pairs not matching phiX were extracted. Picard (version 2.7.1.1)[60] and Samtools (version 1.7)[59] was used to extract reads from the resulting BAM file and sort them by read name, respectively. Next, reads were trimmed with Trimmomatic (version 0.36.3)[62] with sliding window trimming with an average base quality of 20 across 4 bases as cutoff and dropping resulting reads with a residual length < 50. Read pairs, in which one read was dropped according to these rules were dropped altogether. Resulting read pairs were mapped to a

merged FASTA file combining reference genomes of the final filtered taxon list (Supplementary Table 1, Accession numbers in Supplementary Table 16). Subsequently, Samtools (version 1.7)[59] was used to filter only mapped read pairs with a quality of at least 60. Customized scripts were used to generate statistics on the number of mapped reads per species-level taxon in the whole dataset.

In the second alternative strategy, Unicycler (version 0.4.6.0)[80] was used to assemble reads from a merged read database containing all non-human and non-phiX mapped, trimmed read pairs generated as described above for the first alternative, BWA-based strategy. Unicycler (version 0.4.6.0)[80] was run with standard settings. The assembled contigs were then matched to sequences in a combined database consisting of the htgs (downloaded on 04/13/2014), nt (downloaded on 04/17/2014 and wgs (downloaded on 04/20/2014) database using BLAST megablast (beginning with version 2.7.1 and subsequently updated)[75] with an expectation value cutoff of 0.001. Next, customized scripts were used to filter out all contigs with a sequence identity to its matched sequence ≤ 80% and to sum the total alignment length of all remaining contigs by matched sequence template. Finally, for each of the final filtered taxon list (Supplementary Table 1), the matched sequence template representing the species-level taxon with the biggest summed up alignment length was selected.

Next, in order to validate the KRAKEN-based pipeline, the $\log_{10}$ of the number of read pairs assigned to a species-level taxon with KRAKEN (version 1.2.3)[25] , the $\log_{10}$ of read pairs mapped to a taxon with the BWA-based approach and the $\log_{10}$ of the total alignment length of the assembly-based approach were computed for all taxa in the final filtered taxon list (Supplementary Table 1) and compared (Supplementary Table 16). To assess the correlation between the main method and the two tested alternative methods, the Pearson correlation coefficient was calculated.

Finally, in order to assess the concordance between RNA-Seq and WGS experiments performed on the same sample the main pipeline was applied with the same settings to all samples with RNA-Seq and WGS paired data available (n=324). Pearson correlation coefficients of $\log_{10}$ transformed data were calculated for both a combined dataset of all RNA-Seq / WGS pairs and for each sample separately for which RNA-Seq and WGS data was available (n=324).

Assessment of somatic lateral gene transfer

In order to assess the integration of bacterial DNA into human DNA, read pairs with one read matching the human genome and one read matching one of the taxa in the final filtered taxon list (n=27) (Supplementary Table 19) were identified. First, representative bacterial and viral genomes for the final filtered taxon list were downloaded (Accession numbers in Supplementary Table 19). These genomes were merged with the human reference genome (hg1k_v37, downloaded from the 1000 genomes FTP server[56]) into one FASTA file using customized scripts. Second, all read pairs in which only one read of a read pair was mapped to the human genome were filtered using Samtools (version 1.7)[59]. All tumor tissue samples and matched normal samples of all patients in which at least 1000 RPPB matching one of the taxa in the final filtered taxon list were identified in that respective patient's tumor tissue sample (n=79, Supplementary table 20) were included in this analysis. BWA mem (version 0.7.17)[79] with standard settings in paired end mode was used to align all such read pairs to the merged FASTA file of all taxa and the human reference genome. Next, all read pairs that were now divergently mapped were extracted using Samtools (version 1.7)[59] and customized scripts by only including read pairs where one read mapped to one of the included non-human taxa and the other read mapped to a human sequence. Only read pairs with a mapping quality of at least 40 were retained. Customized scripts were used to count and tabulate all divergent

read pairs obtained by taxa and sample, respectively (Supplementary Table 21, Supplementary Table 22). In order to normalize read pairs mapping to putative integration sites (i.e. divergently mapped read pairs as defined above) by correcting for the total number of read pairs matching a taxon with a similar approach (i.e. non-divergently mapped, putatively non-integrated reads), a comparable pipeline was applied to the data used for the main analysis (i.e. both reads in a read pair not mapped to the human genome) of all patients included in the integration analysis (n=79) (Supplementary Table 20). First, the genomes of all taxa in the final filtered taxon list were downloaded (Accession numbers in Supplementary Table 16) and merged without adding any further human sequences into one FASTA file to create a reference genome containing all taxa in the final filtered taxon list. BWA mem (version 0.7.17)[79] with standard settings in paired end mode was used to align these reads to the merged FASTA file of all taxa in the final filtered taxon list. Subsequently, Samtools (version 1.7)[59] was used to filter the aligned data to only include read pairs that mapped as a proper pair to only one taxon with a minimum mapping quality of 60. Samtools (version 1.7)[59] and customized scripts were used to count and tabulate all mapped reads. The putative integration rate of a taxon in either tumor tissue samples or matched normal samples was calculated by dividing the number of divergently mapping read pairs by the number of read pairs mapping as a proper pair to the respective taxon.

Analysis of associations of patient features with identified clusters

Differences in age at diagnosis between patient clusters were first analyzed by ANOVA for each cancer. All results with $p_{anova} \leq 0.1$ are shown separately for each cancer in Figure 4. Such clusters or combinations of clusters were then compared to the other clusters by student t-test.

Differences in the gender distribution between patient clusters were analyzed by chi-square test for each cancer.

In order to analyze possible relationships between the number or type of cancer-associated genetic alterations and presence of specific taxa, all somatic alterations for all patients included in this study were obtained from the ICGC data portal[23,55]. All synonymous mutations were filtered out. Subsequently, only Tier 1 cancer gene census[81] genes that were altered in more than 20 cases were filtered using customized scripts and included in the analysis (Supplementary Table 23).

Differences in the number of genetic alterations in cancer genes between patient clusters were first analyzed by ANOVA for each cancer All results with $p_{anova} \leq 0.1$ are shown separately for each cancer in Figure 4. Such clusters or combinations of clusters were then compared to the other clusters by student t-test.

The Kaplan-Meier method was used to estimate survival curves for each patient cluster in each cancer with available survival data. Differences in survival between patient clusters were analyzed by log rank test.

Associations between patient clusters and alterations in single cancer genes were analyzed for each cancer gene in a cancer that was altered in at least 10 patients in that respective cancer by chi-square test. Clusters or combinations of clusters were then compared to the other clusters by Fisher's exact test.

All calculations were performed with R (beginning with version R 3.3.2. and subsequently updated)[65].

Unbiased analysis of association of patient features with the presence of certain taxa

For this analysis a taxon was considered detected in a patient if at least 100 RPPB matched the respective taxa in the patient's tumor tissue sample. All phages were excluded from the analysis. All included projects were grouped by cancer (Supplementary Table 18). Cancer genes were defined as above.

All calculations were performed with R (beginning with version R 3.3.2. and subsequently updated)[65]. All p-values were corrected for multiple testing using the FDR method to obtain a q-value, which was considered significant if < 0.05.

Survival analysis

First, the Kaplan-Meier method was used to estimate survival curves for each cancer-taxon pair separately that was present in at least 10 patients. Differences in survival between patients with presence or absence of a respective taxon were analyzed using log rank tests, stratified by ICGC project. Additionally, a pan-cancer analysis was performed in the same way, also stratifying by ICGC project.

Association between taxa and patient gender

Associations between presence or absence of a taxa and patient gender were analyzed by Fisher's exact test for each cancer-taxon pair separately that was detected in at least 10 patients. Additionally, a pan-cancer analysis was performed in the same way, using a logistic regression model that included the ICGC project as an independent variable.

Association between taxa and patient age

Associations between presence or absence of a taxon and patient age at diagnosis were analyzed by student t-test for each cancer-taxon pair separately that was present in at least

10 patients. Additionally, a pan-cancer analysis was performed in the same way, using a linear regression model that was stratified by ICGC project.

Association between taxa and number of genetic alterations in cancer genes

Associations between presence or absence of a taxon and the number of non-synonymous genetic alterations in cancer gene consensus[81] genes of a patient were analyzed by student t-test for each cancer-taxon pair separately that was present in at least 10 patients. Additionally, a pan-cancer analysis was performed in the same way, using a linear regression model that was stratified by ICGC project.

Association between taxa and specific genetic alterations

Associations between presence or absence of a taxon and non-synonymous alterations in one of the cancer gene consensus[81] genes of a patient were analyzed by Fisher exact test for each cancer-taxon pair separately that was detected in at least 10 patients. Additionally, a pan-cancer analysis was performed in the same way, using a logistic regression model that included the ICGC project as an independent variable.

Analysis of differential gene expression

Reads per kilobase of transcript, per million mapped reads (RPKM) data was downloaded from http://dcc.icgc.org/pcawg for all available tumor tissue samples. Ensemble gene ID was substituted by the standard Human Genome Organization (HUGO) Gene Nomenclature Committee (HGNC) symbol downloaded from http://genenames.org/download/custom and the RPKM data was then linked to the identified species-level taxa in each sample using R (beginning with version R 3.3.2. and subsequently updated)[65]. sRAP[82] was used to normalize RPKM values, perform quality control, differential gene expression analysis and to identify

pathways that are differentially expressed. For these analyses, each cancer was analyzed separately and patients that had more than 100 RPPB matching one species-level taxon in the final filtered taxon list were compared with those who had not. Differential gene expression analysis was performed for all taxa that were detected with more than 100 RPPB in at least five patients and RNA-seq data available (Supplementary Table 24). Next, sRAP[82] was used to perform bidirectional functional enrichment of gene expression data to identify pathways up- or downregulated between patients with or without presence of a taxon. Briefly, the distribution of activation versus inhibition t-test statistics for all samples associated or not associated with a specific taxon was compared using ANOVA and corrected for multiple testing using the FDR method. For details please refer to the original description of BD-Func[83]. A gene set was considered functionally enriched, if $q<0.05$. Gene sets likely not relevant for the respective cancer were excluded and gene sets provided with sRAP[82] were reduced to gene ontology (GO) gene sets[84].

FIGURE LEGENDS

Figure 1: Overview over sample characteristics and identified taxa

A, Sample distribution by project. B, sample distribution by age group. C, sample distribution by gender. D, distribution of read pairs matching any species-level taxa by project. E, distribution of read pairs matching any species-level taxa by sample type. F, species-level taxa detected in at least 10 samples (detection limit 100 read pairs per billion (RPPB)) color-coded by project. G, average RPPB detected across all species-level taxa by project and sample type. Bars show mean of samples and error bars show standard error of mean. H, average RPPB detected by species-level taxa and sample type. I, average RPPB detected for all species-level taxa identified as likely tumor associated after filtering by sample type. J, species-level taxa identified as likely tumor associated after filtering (detection limit 100 RPPB) color-coded by project.

Figure 2: Heatmap of all taxa detected in all samples

Log2-transformed read pairs per billion (RPPB) of all taxa in all samples. Taxa were hierarchically clustered using Pearson correlation as a distance measure with average-linkage. Samples were hierarchically clustered within each project and type subgroup using Pearson correlation as a distance measure with average-linkage.

Figure 3: Patient clusters defined by detected taxa can be identified across all patients and cancer-specific subgroups

A, t-SNE visualization of all tumor-tissue samples color coded by project using the $\log_2$-transformed read pairs per billion (RPPBs) of all detected non-phage taxa as input variables. B-H, t-SNE visualizations of single cancer subgroup tumor-tissues color coded by k-means

cluster (Extended data figure 4) using the log_2-transformed read pairs per billion (RPPBs) of all detected non-phage taxa as input variables.

Figure 4: Patient clusters defined by detected taxa associate with patient characteristics

A, association of CLL patient clusters (1: no specific association, 2: Human Mastadenovirus C, 3: Gordonia polyisoprenivorans) with age (p_{anova}=0.0743). B, survival by cluster in CLL (p(1 vs. other)=0.0246). C, Binet stage depending on detection of Gordonia polyisoprenivorans ($p_{Fischer}$ = 0.0252). D, TP53 alteration frequency by cluster in CLL (p_{Fisher}(cluster 3 vs. other)=0.0335). E, number of cancer consensus gene alterations by cluster (1: no specific association, 2: Bifidobacterium dentium, 3: Human Herpesvirus 5) in esophageal cancer (p_{anova}=0.0858). F, Kaplan-Meier survival curves for each cluster in esophageal cancer (p(1 vs. other)= 0.0409). G, association of liver cancer patient clusters (1: Hepatitis B virus, 2: Pseudomonas sp. and Serratia sp., 3: no specific associations, 4: Parvibaculum lavamentivorans and Human Herpesvirus 5 in addition to taxa from cluster 2) with age (p_{anova}=0.0015). H, RNF21 alteration frequency by cluster in liver cancer ($p_{Fischer}$ = 0.0121). I, KMT2C alteration frequency by cluster (1: no specific associations, 2: Cupriavidus metallidurans, 3: no specific associations, 4: Methylobacterium populi, 5: Pseudomonas protegens) in pancreatic cancer (p_{Fisher}=0.0308). J, CDKN2A alteration frequency by cluster in pancreatic cancer (p_{Fisher}=0.0124). K, RNF21 alteration frequency by cluster in pancreatic cancer (p_{Fisher}RNF21=0.0107). L, association of indicated taxa with age in prostate cancer (p_{adj} between 0.0015 and 0.0420). M, association of prostate cancer patient clusters (1: no specific association, 2: Gluconobacter oxydans and Rhodopseudomonas palustris, 3: Pseudomonas sp. TKP, 4: no specific associations, 5: Thauera sp. MZ1T, Cupriavidus metallidurans and Pseudomonas mendocina) with age (p_{anova}=0.00994). N, association between detected amount of Propionibacterium acne DNA and number of cancer consensus

gene alterations (p_{adj}=0.0041). O, Kaplan-Meier survival analysis of Ralstonia pickettii detection status in renal cancer (p_{adj}=0.035). P, PBRM1 alteration frequency by cluster (1: no specific association, 2: Serratia marcescens) in renal cancer (p_{Fisher}=0.0723). Q, association of Pseudomonas sp. TKP detection with age in chronic myeloid dysplasia (p_{adj}=0.039). For all: The midline of the boxplots shows the median, the box borders show upper and lower quartile, the whiskers show 5th and 95th percentiles and the dots outliers.

Figure 5: Differential gene expression and pathway analysis of chronic lymphocytic leukemia patients

A, heatmap of all differentially expressed genes (q<0.05) in tumor tissue samples of chronic lymphocytic leukemia (CLL) patients with (green) and without (orange) detection of Gordonia polyisoprenivorans. Dendrograms show clustering with complete linkage and Euclidian distance measure. B, boxplots of the distribution of activating versus inhibitory gene t-test statistics for the indicated pathway is shown for tumor tissue samples of CLL patients with (+, n=23)) and without (-, n=49) detection of Gordonia polyisoprenivorans. The midline of the boxplot shows the median, the box borders show upper and lower quartile and the whiskers the maximum and minimum test statistic. A, heatmap of all differentially expressed genes (q<0.05) in tumor tissue samples of CLL patients with (green) and without (orange) detection of Human Mastadenovirus C.. D, boxplots of the distribution of activating versus inhibitory gene t-test statistics for the indicated pathway is shown for tumor tissue samples of CLL patients with (+, n=7)) and without (-, n=65) detection of Human Mastadenovirus C. The midline of the boxplot shows the median, the box borders show upper and lower quartile and the whiskers the maximum and minimum test statistic. Dendrograms show clustering with complete linkage and Euclidian distance measure.

Extended Data Table 1: Included patients and samples

Overview of all included patients and samples.

Extended Data Figure 2: Validation of pipeline and analytical approach

A, mean read pairs per billion (RPPB) detected for indicated species in blood derived and lymphoblastoid cell line 1000 Genome samples sorted by mean of blood derived samples. B, proportion of non-human read pairs matching the indicated taxon of read pairs matching any species-level taxon for each external validation sample. C-E, comparison of BWA mapped reads in Kraken matched read pairs. Each dot represents one species-level taxon (n=27). The line represents the best-fitted line (log-log linear regression). The dotted lines depict the 95% confidence interval. Pearson correlation coefficients (log-log) are shown with two-sided p-values. (C) shows all samples (n=27), (D) only bacterial taxa (n=22) and (E) only viral taxa (n=5). F, comparison of assembled read length and Kraken matched read pairs. Each dot represents one species-level taxon (n=27). The line represents the best-fitted line (log-log linear regression). The dotted lines depict the 95% confidence interval. Pearson correlation coefficients (log-log) are shown with two-sided p-values. G, comparison of Kraken matched read pairs in RNA-seq and WGS data of the same sample. Each dot represents one species-level taxon in one sample with both RNA-seq and WGS data available. The line represents the best-fitted line (log-log linear regression). Pearson correlation coefficients (log-log) are shown with two-sided p-values. H, plot of Pearson correlation coefficient (log-log) distribution of all samples with both RNA-seq and WGS data available. Each dot represents the Pearson correlation coefficient within a single sample. I, comparison of 10% subsample and full dataset. Each dot represents one species-level taxon in one sample for which both the full and the subsampled dataset has been analyzed and

indicates the absolute read count identified in both samples. The line represents the best-fitted line (log-log linear regression). Pearson correlation coefficients (log-log) are shown with two-sided p-values. J, Ratio of absolute read counts in the full sample to the 10% subsample for 4 selected taxa. The mean ratio of all samples in which the respective taxon was detected is indicated by the symbol and the error bars indicate the standard error of the mean. The dotted line shows the expected ratio of 10. K, comparison of tumor tissue and matched normal by patient and taxon. Each dot represents one species-level taxon in one patient with both tumor tissue and matched normal analyzed and indicates the RPPB in both samples. The line represents the best-fitted line (log-log linear regression). Pearson correlation coefficients (log-log) are shown with two-sided p-values.

Extended Data Figure 3: Alpha diversity

A, counts of 1000 Genome samples by species-level richness. B, counts of tumor tissue samples by species-level richness color-coded by project. C, counts of matched normal samples by species-level richness color-coded by project. D, comparison of richness between projects and sample type. Bars show mean and error bars standard deviation. N in brackets indicates total sample number for each project.

Extended Data Figure 4: Coverage distribution for all likely tumor-associated species-level taxa

Coverage distribution across each species-level taxon identified as likely tumor associated.

Extended Data Figure 5: Flow chart of taxa filtering strategy

Flow chart of filtering strategy to derive likely tumor-associated species-level taxa.

Extended Data Figure 6: Heatmap of final filtered taxon list

Log_2-transformed read pairs per billion (RPPB) of all species-level taxa identified as likely tumor associated after filtering in all samples. Taxa were hierarchically clustered using Pearson correlation as a distance measure with average-linkage. Samples were hierarchically clustered within each project and type subgroup using Pearson correlation as a distance measure with average-linkage.

Extended Data Figure 7: Heatmaps of likely tumor-associated taxa for all cancers with discernible clusters

A-F, log_2-transformed read pairs per billion (RPPB) of all species-level taxa identified as likely tumor associated and detected after filtering in all tumor-tissues of the indicated cancer. Results of K-means clustering of samples are shown.

Extended Data Figure 8: Heatmaps of likely tumor-associated taxa for all cancers without discernible clusters

A-D, log_2-transformed read pairs per billion (RPPB) of all species-level taxa identified as likely tumor associated and detected after filtering in all tumor-tissues of the indicated cancer. Results of K-means clustering of samples are shown.

Extended Data Figure 9: Analysis of host integration

A, integration rate by species for tumor tissue and matched normal sample. B, difference in integration rates between bacterial and viral taxa ($p<0.0001$, Wilcoxon rank-sum test, two-tailed). The midline of the boxplot shows the median, the box borders show upper and lower quartile, the whiskers show 5th and 95th percentiles and the dots outliers of species-specific integration rates in tumor tissue or matched normal samples. C, difference in integration rate between tumor tissue and matched normal samples ($p=0.0009$, Wilcoxon signed-rank

test, two-tailed).). The midline of the boxplot shows the median, the box borders show upper and lower quartile, the whiskers show 5th and 95th percentiles and the dots outliers of species-specific integration rates.

Extended Data Figure 10: „Elbow method“ to determine k for k-mean clustering

A-J, plot of reducing within group sum of squares for increasing k (number of clusters) in k-means clustering (Extended data figure 4, Extended data figure 5) of log_2-transformed read pairs per billion (RPPB) of all species-level taxa identified as likely tumor associated and detected after filtering in all tumor-tissues for each indicated cancer.

FIGURES

Figure 1

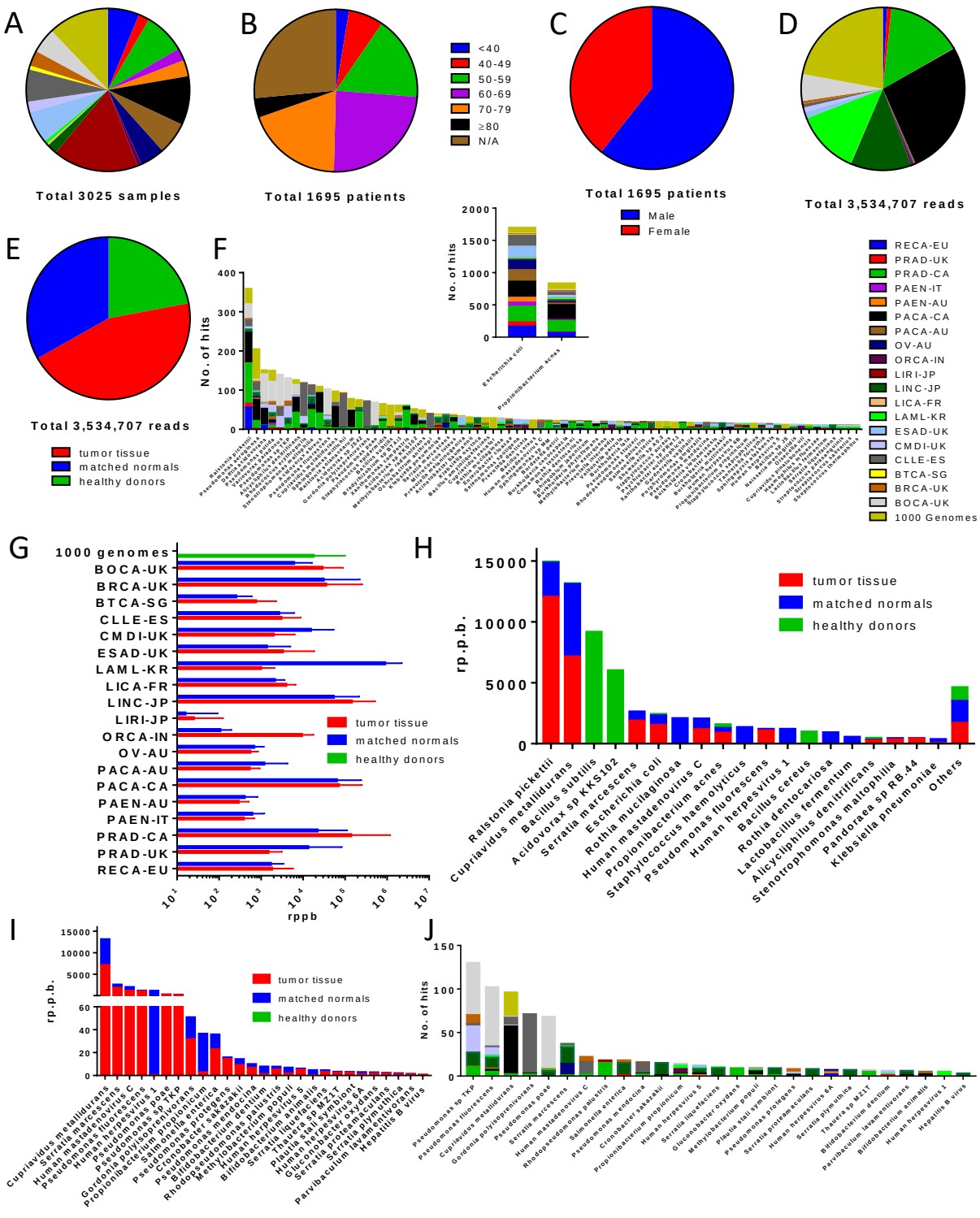

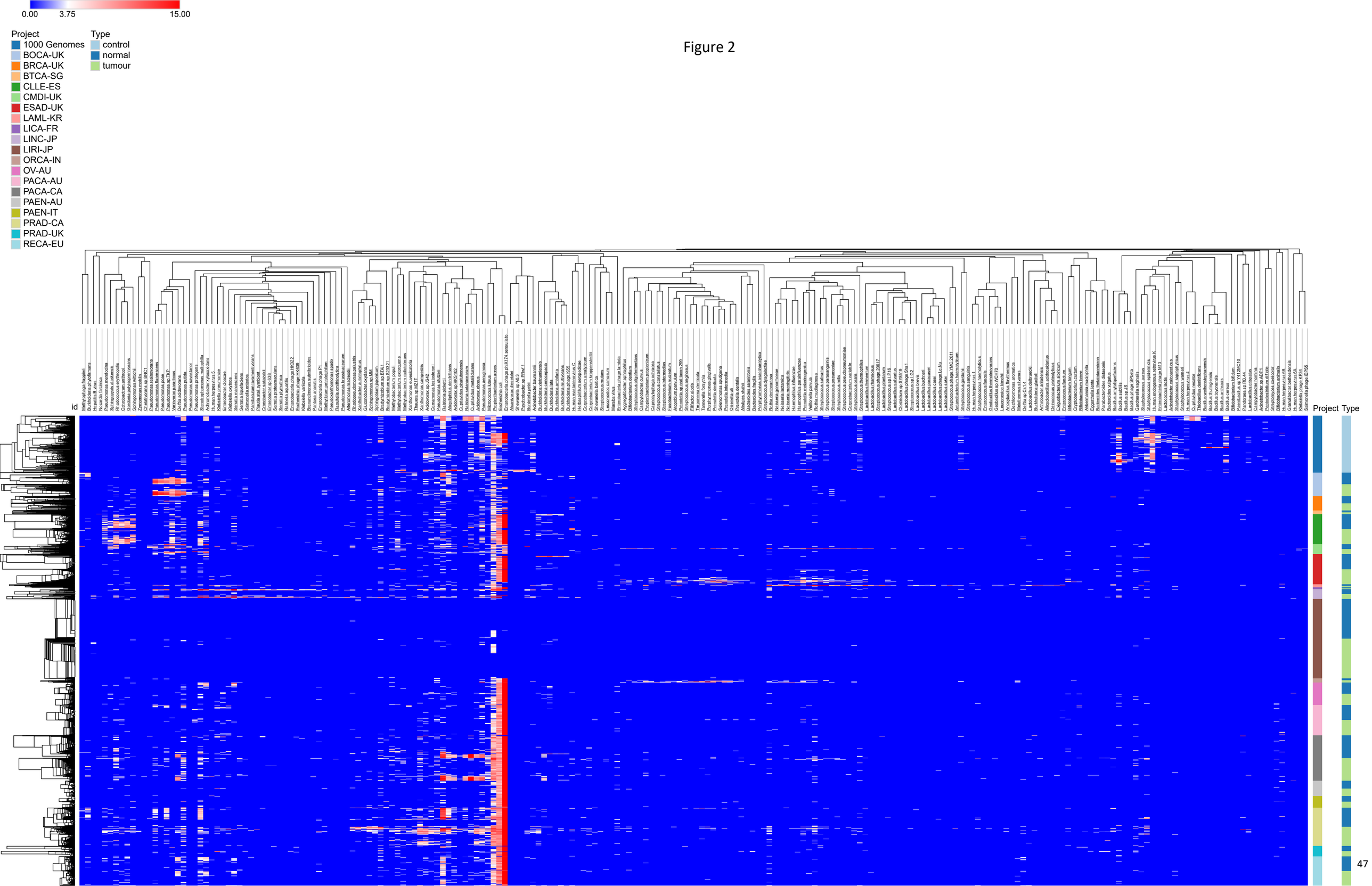
0.00
3.75
15.00
Project
1000 Genomes
BOCA-UK
BRCA-UK
BTCA-SG
CLLE-ES
CMDI-UK
ESAD-UK
LAML-KR
LICA-FR
LINC-JP
LIRI-JP
ORCA-IN
OV-AU
PACA-AU
PACA-CA
PAEN-AU
PAEN-IT
PRAD-CA
PRAD-UK
RECA-EU
Type
control
normal
tumour
id
Project
Type

Figure 2

Figure 3

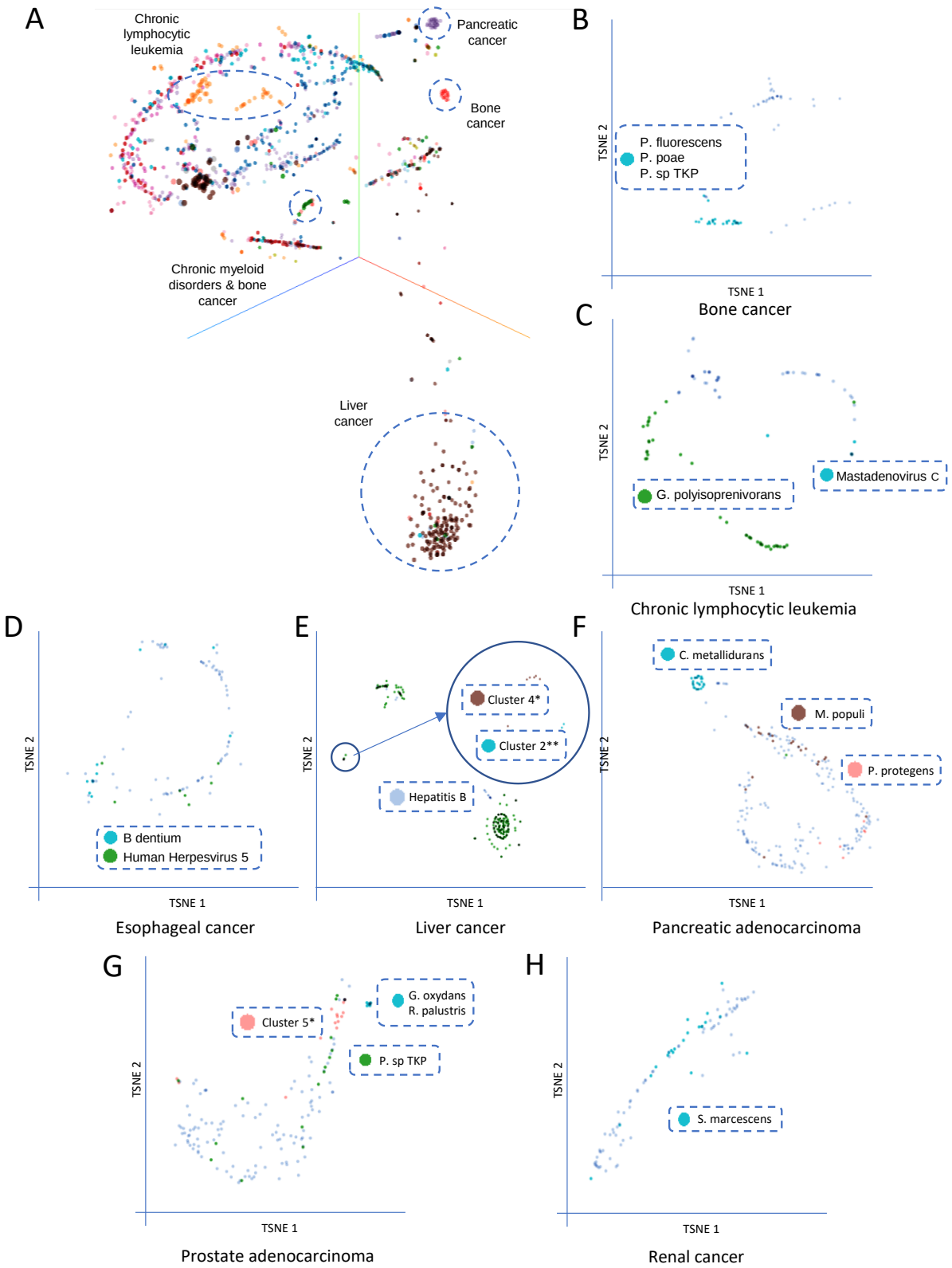
A
Chronic lymphocytic leukemia
Pancreatic cancer
Bone cancer
Chronic myeloid disorders & bone cancer
Liver cancer
B
TSNE 2
P. fluorescens
P. poae
P. sp TKP
TSNE 1
Bone cancer
C
TSNE 2
Mastadenovirus C
G. polyisoprenivorans
TSNE 1
Chronic lymphocytic leukemia
D
TSNE 2
B dentium
Human Herpesvirus 5
TSNE 1
Esophageal cancer
E
TSNE 2
Cluster 4*
Cluster 2**
Hepatitis B
TSNE 1
Liver cancer
F
TSNE 2
C. metallidurans
M. populi
P. protegens
TSNE 1
Pancreatic adenocarcinoma
G
TSNE 2
Cluster 5*
G. oxydans
R. palustris
P. sp TKP
TSNE 1
Prostate adenocarcinoma
H
TSNE 2
S. marcescens
TSNE 1
Renal cancer

Figure 4

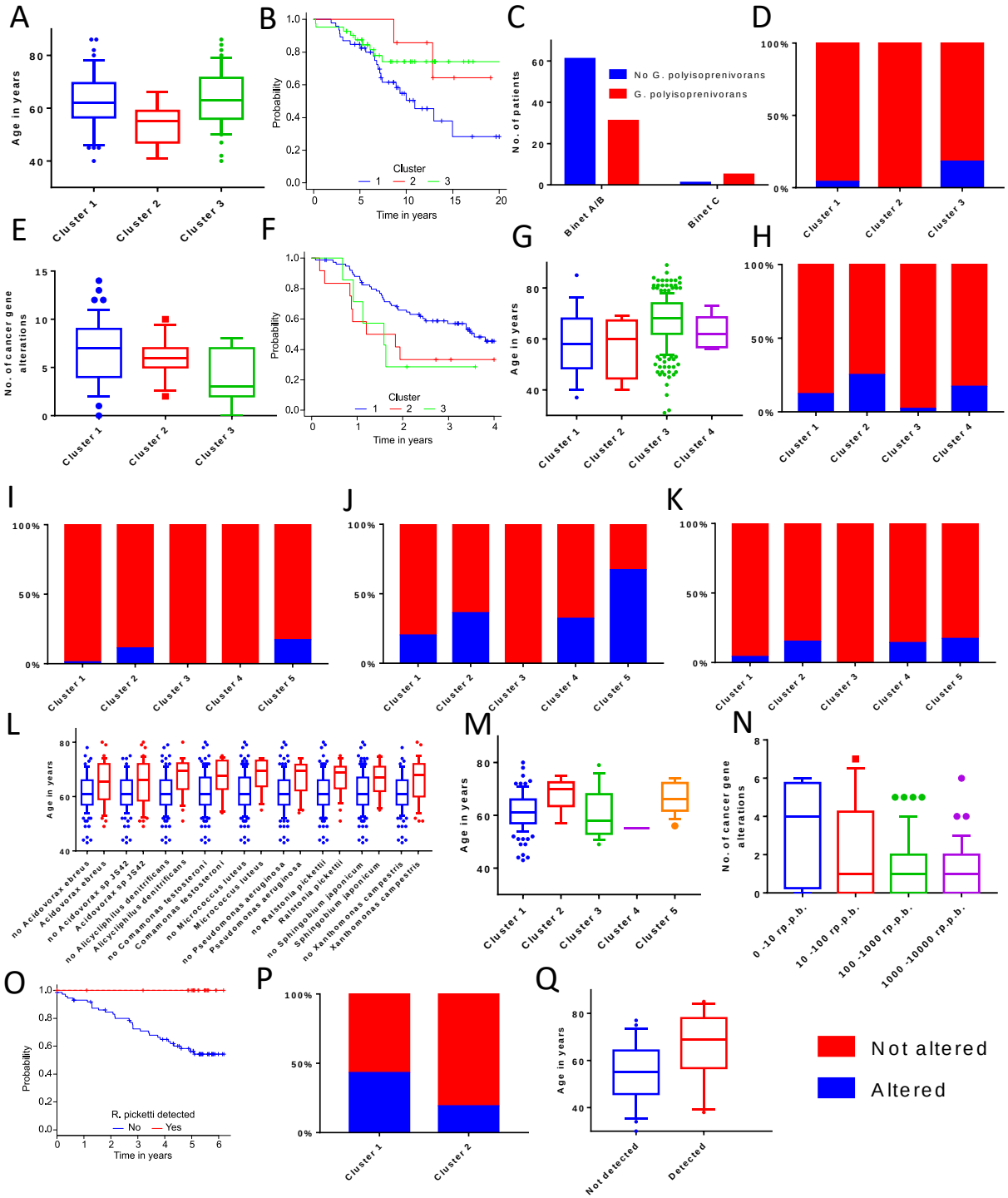
A
Age in years
Cluster 1
Cluster 2
Cluster 3
B
Probability
Time in years
Cluster
1
2
3
C
No. of patients
No G. polyisoprenivorans
G. polyisoprenivorans
Binet A/B
Binet C
D
100%
50%
0%
E
No. of cancer gene alterations
F
G
Cluster 4
H
I
Cluster 5
J
K
L
no Acidovorax ebreus
Acidovorax ebreus
no Acidovorax sp JS42
Acidovorax sp JS42
no Alicycliphilus denitrificans
Alicycliphilus denitrificans
no Comamonas testosteroni
Comamonas testosteroni
no Micrococcus luteus
Micrococcus luteus
no Pseudomonas aeruginosa
Pseudomonas aeruginosa
no Ralstonia picketti
Ralstonia picketti
no Sphingobium japonicum
Sphingobium japonicum
no Xanthomonas campestris
Xanthomonas campestris
M
N
0 -10 rp.p.b.
10 -100 rp.p.b.
100 -1000 rp.p.b.
1000 -10000 rp.p.b.
O
R. picketti detected
No
Yes
P
Q
Not detected
Detected
Not altered
Altered

Figure 5

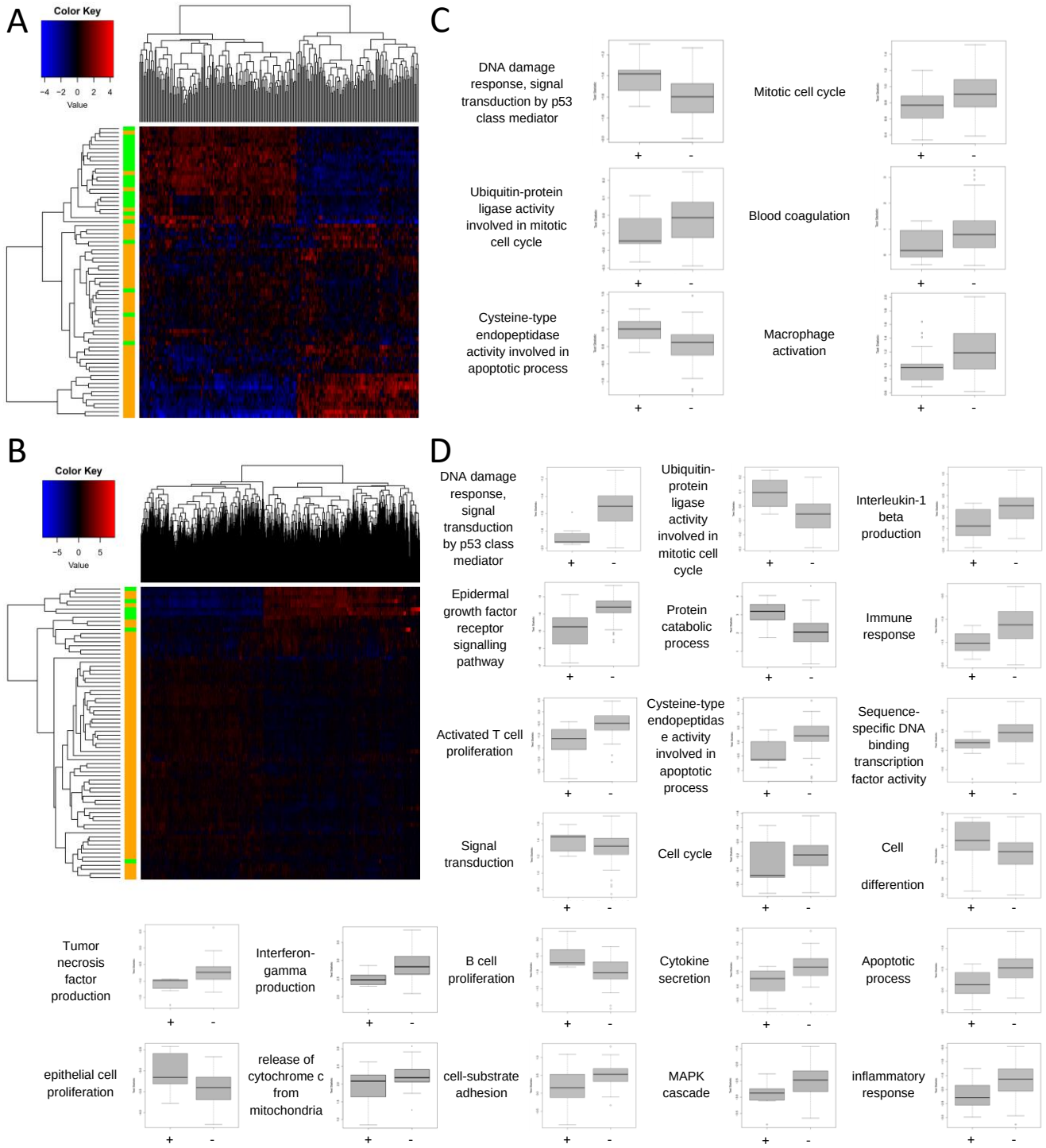
A
Color Key
−4 −2 0 2 4
Value
B
Color Key
−5 0 5
Value
C
DNA damage response, signal transduction by p53 class mediator
Mitotic cell cycle
Ubiquitin-protein ligase activity involved in mitotic cell cycle
Blood coagulation
Cysteine-type endopeptidase activity involved in apoptotic process
Macrophage activation
D
DNA damage response, signal transduction by p53 class mediator
Ubiquitin-protein ligase activity involved in mitotic cell cycle
Interleukin-1 beta production
Epidermal growth factor receptor signalling pathway
Protein catabolic process
Immune response
Activated T cell proliferation
Cysteine-type endopeptidase activity involved in apoptotic process
Sequence-specific DNA binding transcription factor activity
Signal transduction
Cell cycle
Cell differention
Tumor necrosis factor production
Interferon-gamma production
B cell proliferation
Cytokine secretion
Apoptotic process
epithelial cell proliferation
release of cytochrome c from mitochondria
cell-substrate adhesion
MAPK cascade
inflammatory response
+
-

Extended Data Table 1

						Phage			Virus			Bacteria			All		
Project	**healthy normals**	**matched control samples**	**tumor-tissue samples**	**Project total samples**	**Project total reads in bn**	**healthy normals**	**matched control samples**	**tumor-tissue samples**	**healthy normals**	**matched control samples**	**tumor-tissue samples**	**healthy normals**	**matched control samples**	**tumor-tissue samples**	**healthy normals**	**matched control samples**	**tumor-tissue samples**
1000 Genomes	365			365	85.85	444			13,725			764,787			778,956		
BOCA-UK		76	76	152	193.74		1	0		25	0		22,502	166,820		22,528	166,820
BRCA-UK		46	46	92	121.42		3	3		4,602	10,404		2,730	1,800		7,335	12,207
BTCA-SG		12	12	24	44.30		0	0		0	0		259	554		259	554
CLLE-ES		97	97	194	179.15		3	4		515	676		11,548	13,256		12,066	13,936
CMDI-UK		32	32	64	84.55		23	20		2	2		28,464	4,759		28,489	4,781
ESAD-UK		97	97	194	343.24		61	5		42	140		9,258	33,838		9,361	33,983
LAML-KR		10	10	20	20.42		173	2		87,268	29		358,442	515		445,883	546
LICA-FR		6	6	12	17.85		0	0		2	0		1,065	1,584		1,067	1,584
LINC-JP		31	31	62	102.88		104	239		37	140		99,733	324,055		99,874	324,434
LIRI-JP		256	256	512	641.41		0	0		3	21		182	376		185	397
ORCA-IN		13	13	26	41.72		0	0		0	2		80	12,589		80	12,591
OV-AU		73	73	146	220.69		11	16		30	24		3,316	3,394		3,357	3,434
PACA-AU		97	97	194	348.55		13	18		145	97		7,142	6,348		7,300	6,463
PACA-CA		147	147	294	337.77		32	19		31	83		377,496	566,397		377,559	566,499
PAEN-AU		49	49	98	165.19		4	4		102	151		1,128	1,371		1,234	1,526
PAEN-IT		37	37	74	82.95		0	0		7	4		733	909		740	913
PRAD-CA		124	124	248	269.85		21	35		8	61		115,213	412,634		115,242	412,730
PRAD-UK		33	33	66	111.30		50	6		3	2		24,961	5,601		25,014	5,609
RECA-EU		94	94	188	377.53		2	4		49	50		15,442	13,624		15,493	13,678
TOTAL	**365**	**1,330**	**1,330**	**3,025**	**3,790.34**	**444**	**501**	**375**	**13,725**	**92,871**	**11,886**	**764,787**	**1,079,694**	**1,570,424**	**778,956**	**1,173,066**	**1,582,685**

Extended Data Figure 2

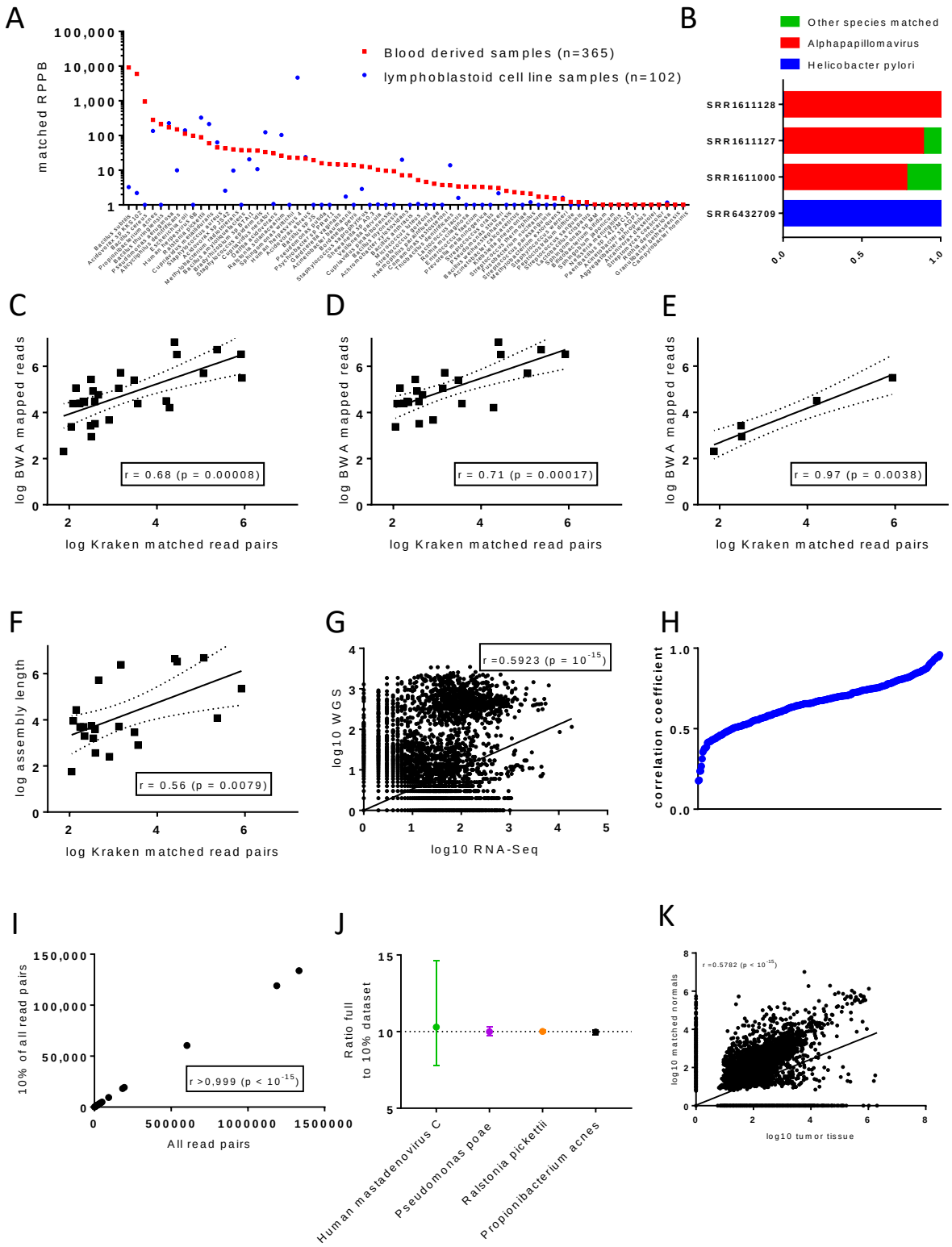

Extended Data Figure 3

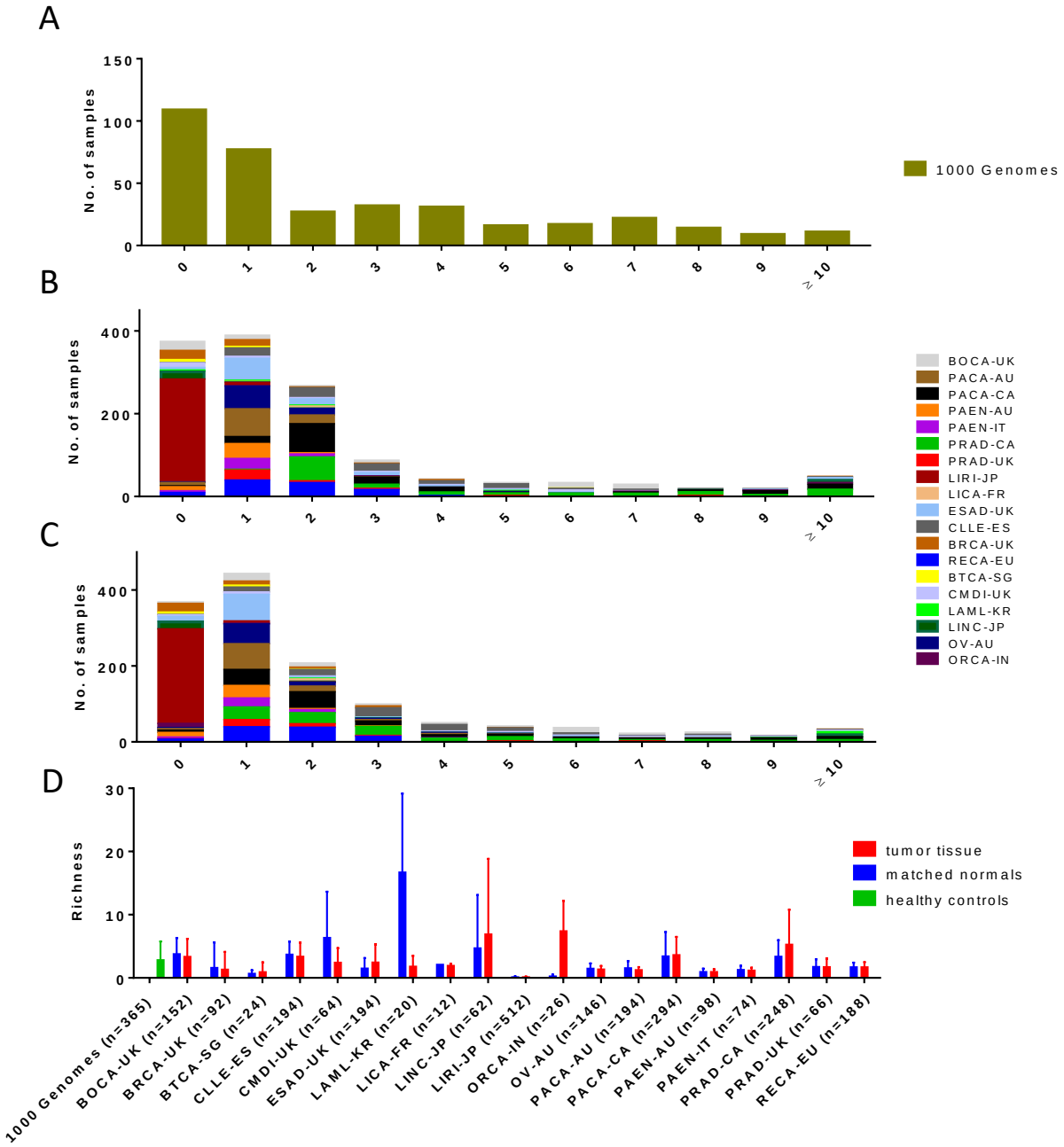

Extended Data Figure 4

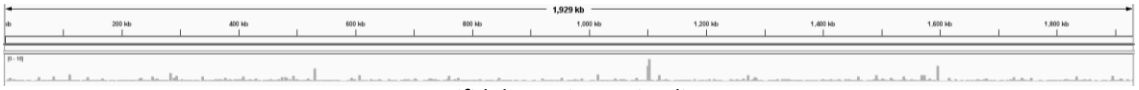

Bifidobacterium animalis

Bifidobacterium dentium

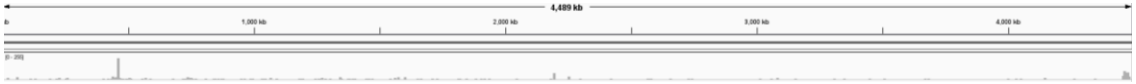

Cronobacter sakazakii

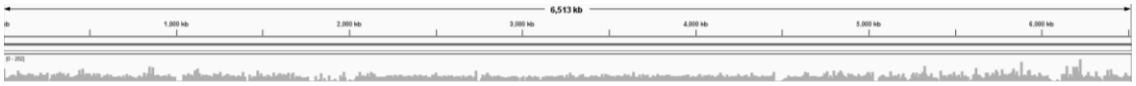

Cupriavidus metallidurans

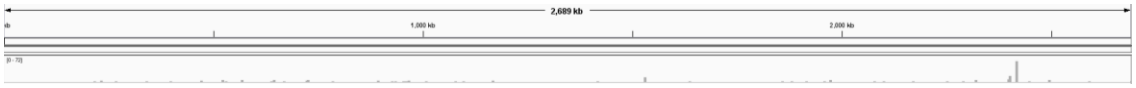

Gluconobacter oxydans

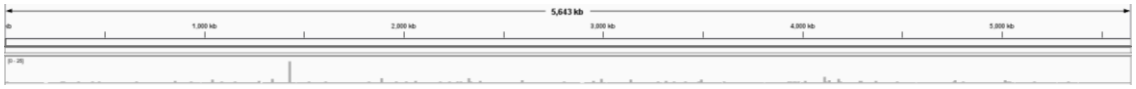

Gordonia polyisoprenivorans

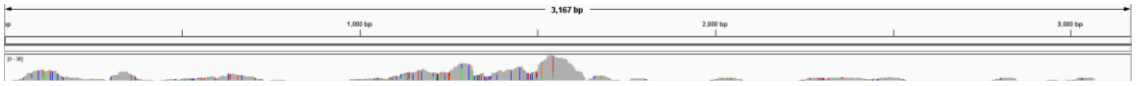

Hepatitis B virus

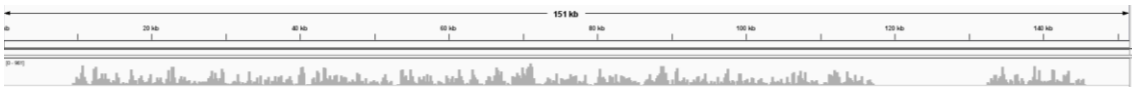

Human herpesvirus 1

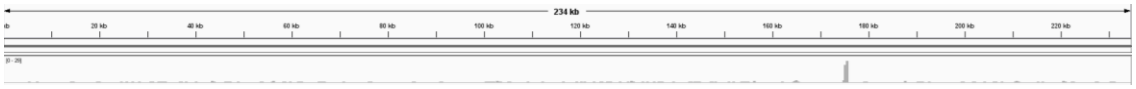

Human herpesvirus 5

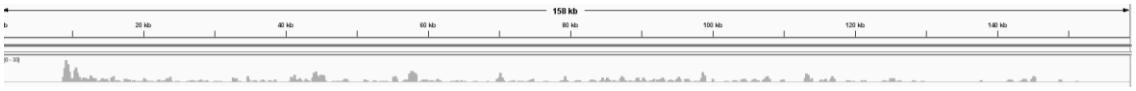

Human herpesvirus 6A

Human mastadenovirus C

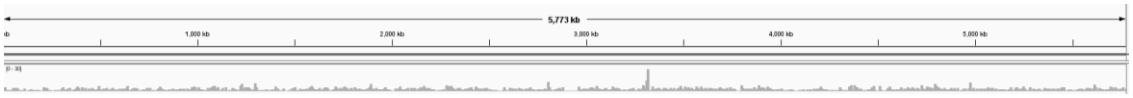

Methylobacterium populi

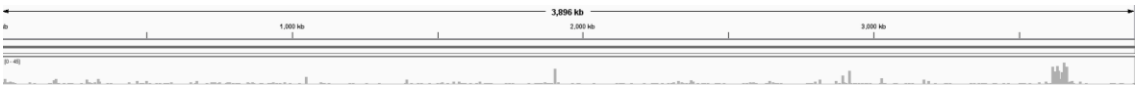

Parvibaculum lavamentivorans

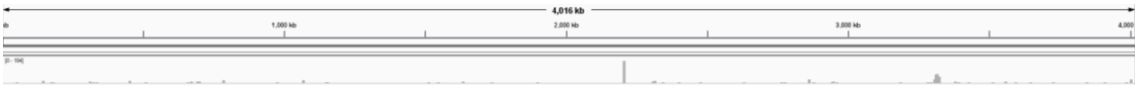

Plautia stali symbiont

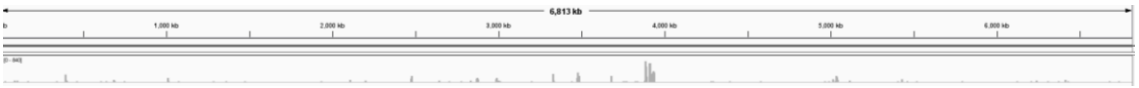

Pseudomonas fluorescens

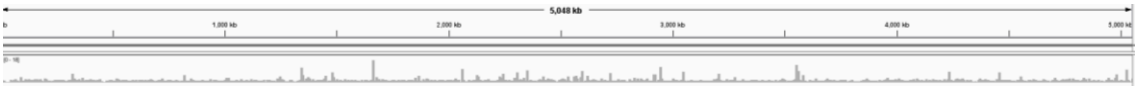

Pseudomonas mendocina

Pseudomonas poae

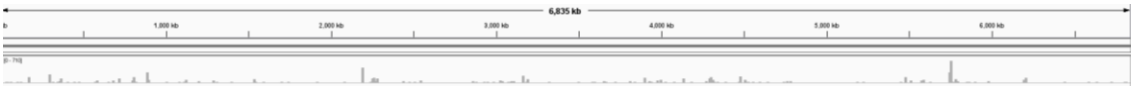

Pseudomonas protegens

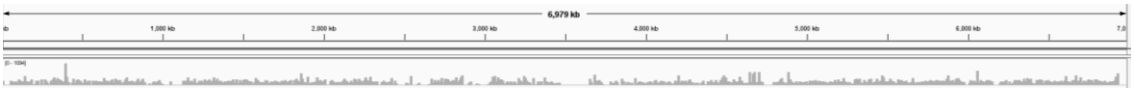

Pseudomonas sp. TKP

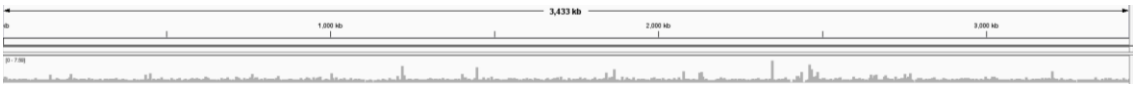

Pseudopropionibacterium propionicum

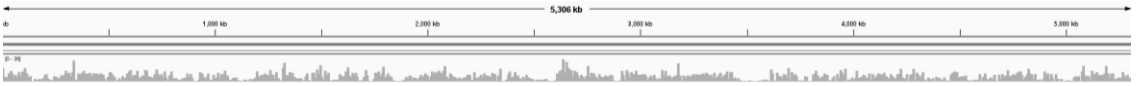

Rhodopseudomonas palustris

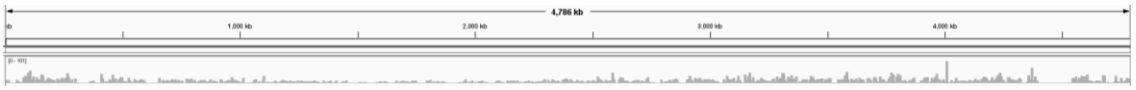

Salmonella enterica subsp. enterica serovar Typhi

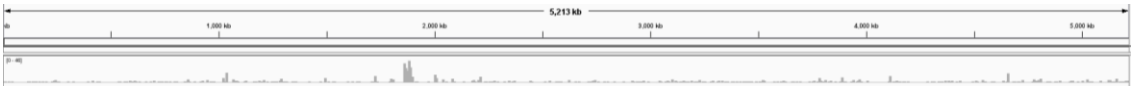

Serratia liquefaciens

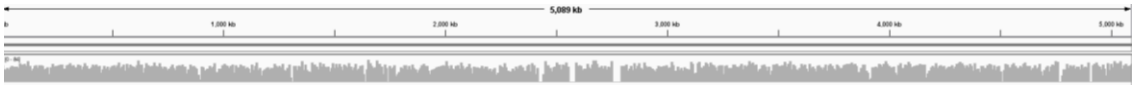

Serratia marcescens subsp. marcescens

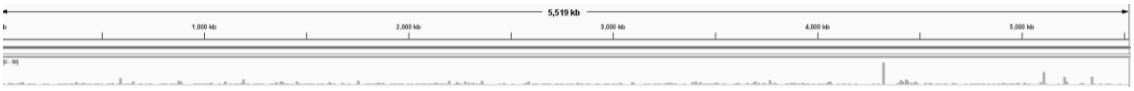

Serratia plymuthica

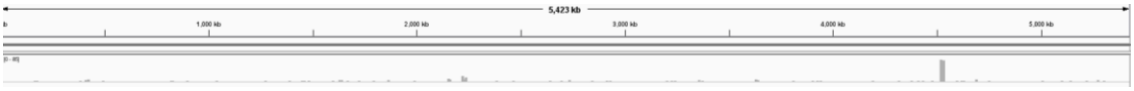

Serratia proteamaculans

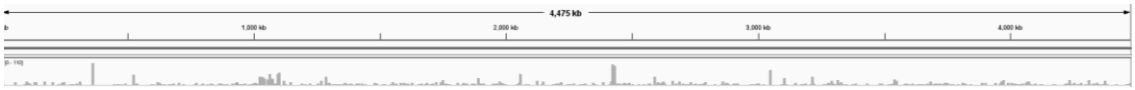

Thauera sp. MZ1T

Extended Data Figure 5

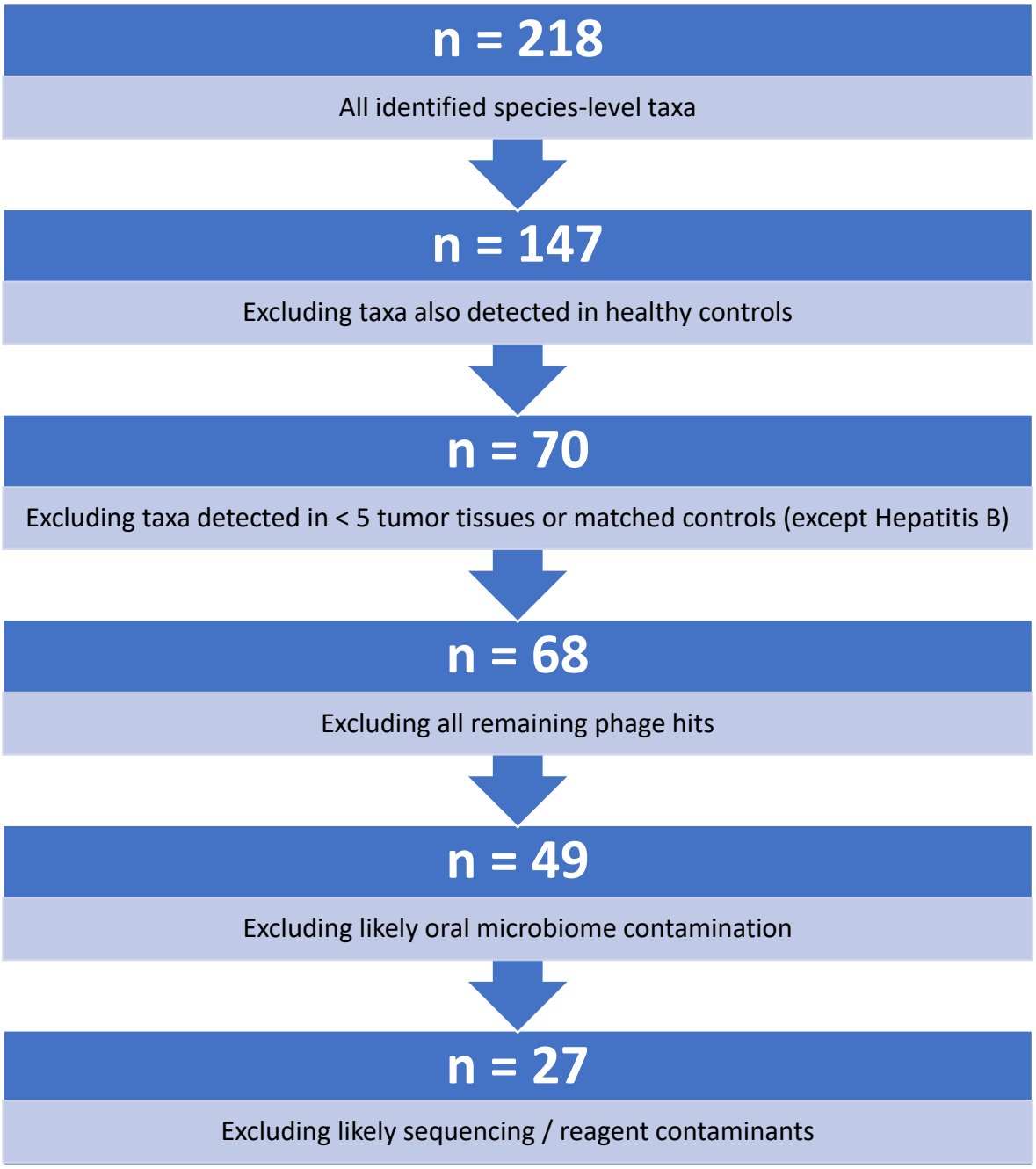

Extended Data Figure 6

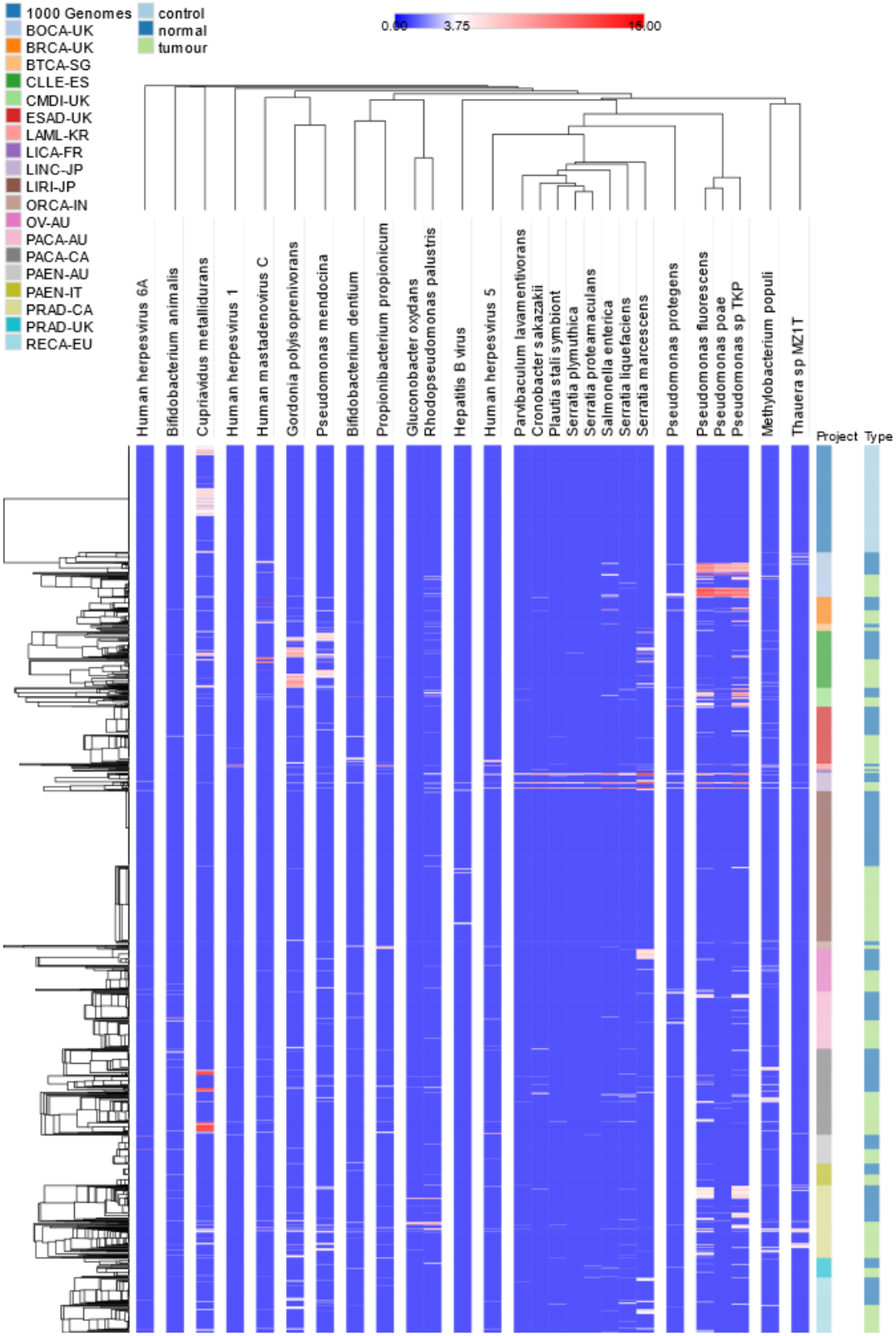

Extended Data Figure 7

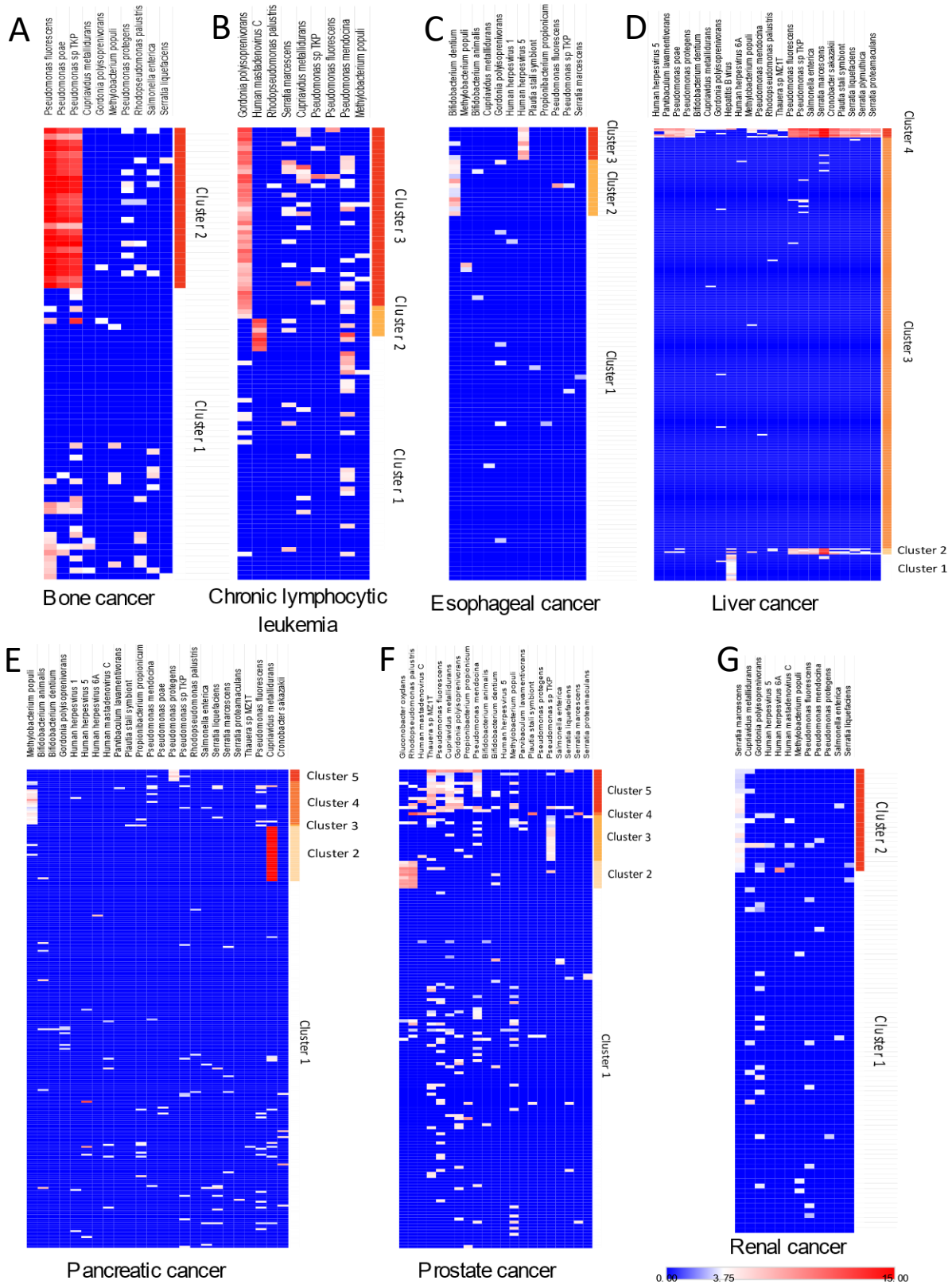

Extended Data Figure 8

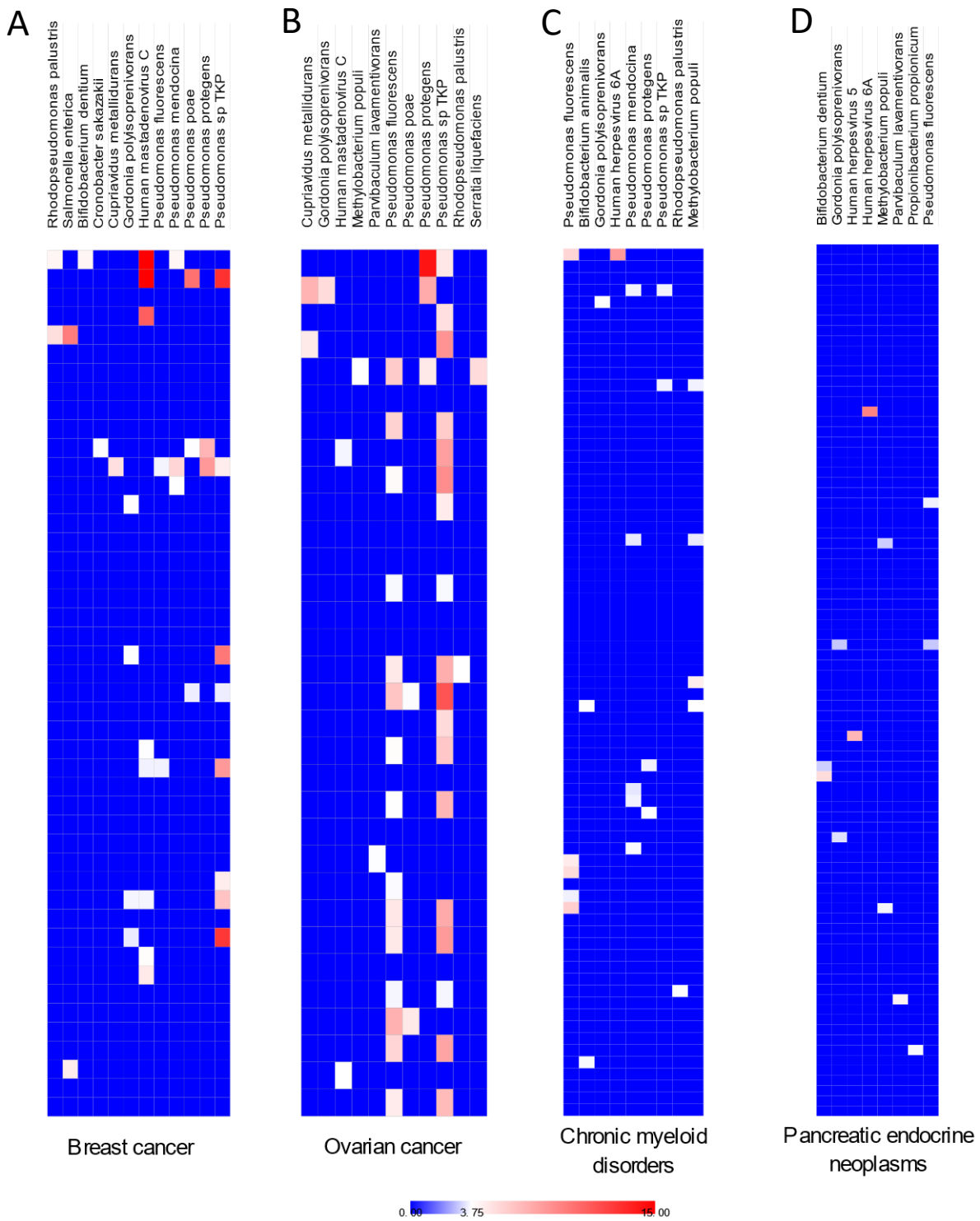

Extended Data Figure 9

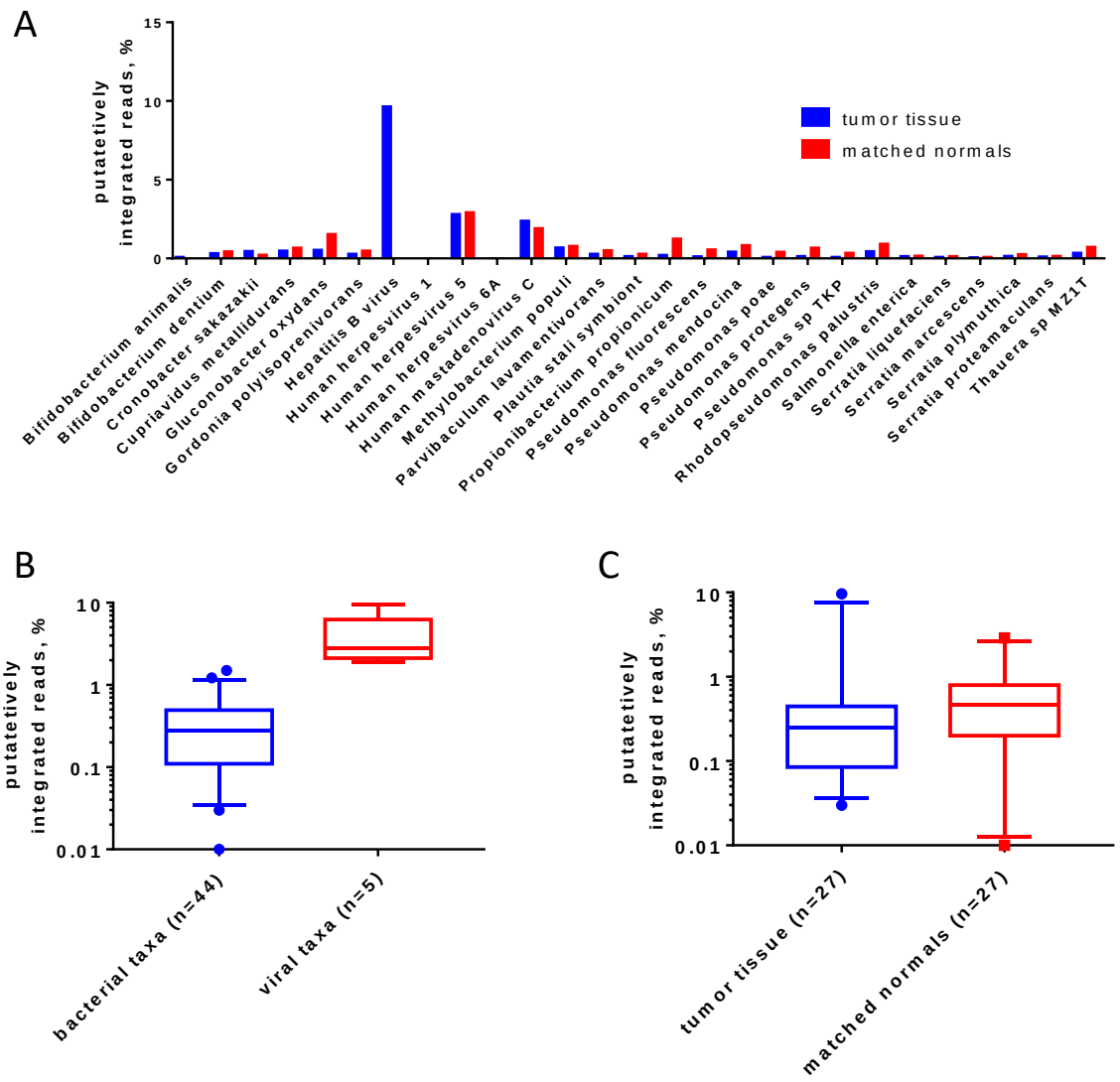

Extended Data Figure 10

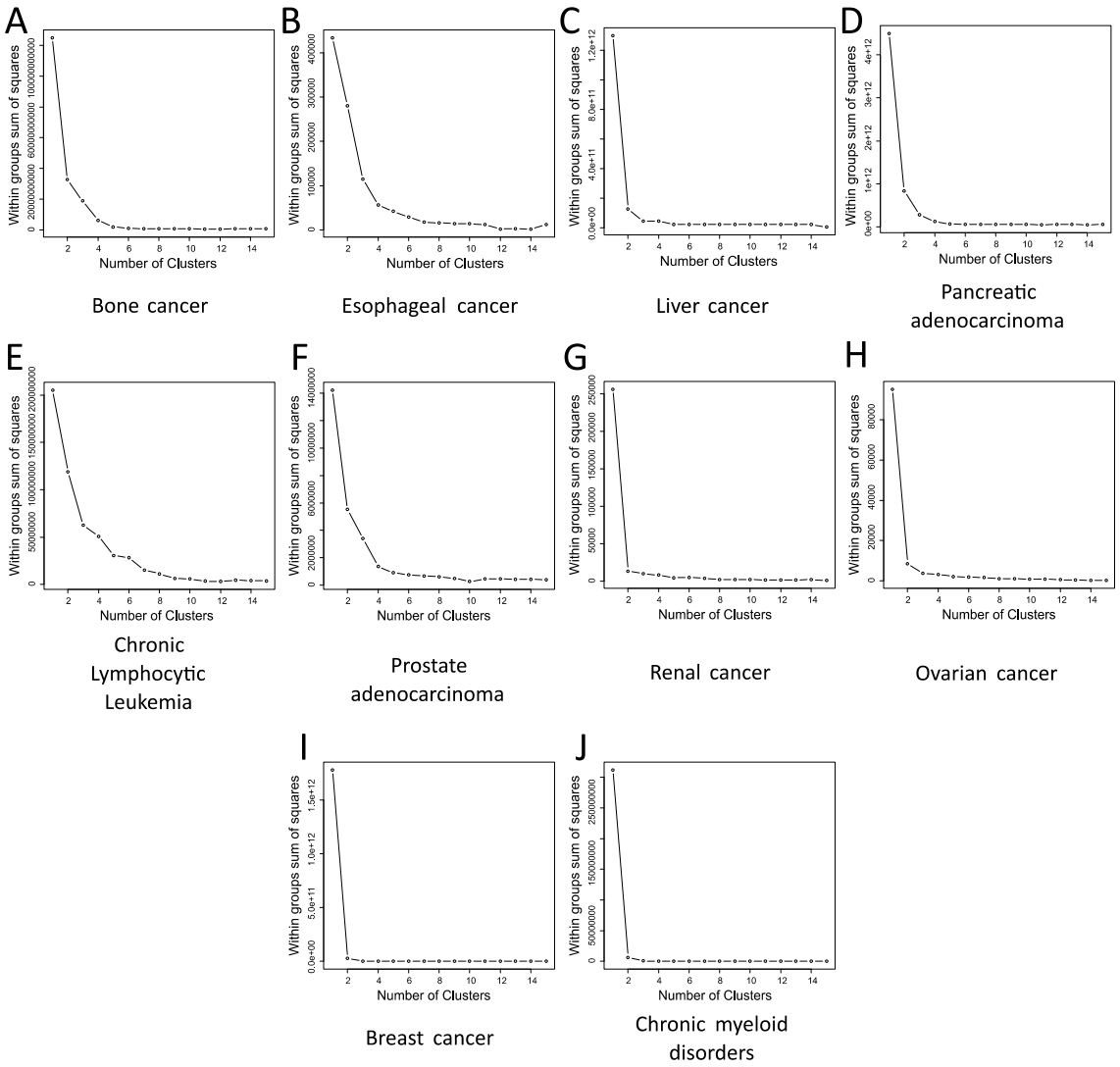

REFERENCES

1. Schwabe, R. F. & Jobin, C. The microbiome and cancer. *Nat. Rev. Cancer* **13**, 800–12 (2013).

2. Goodman, B. & Gardner, H. The microbiome and cancer. *J. Pathol.* **244**, 667–676 (2018).

3. zur Hausen, H. Papillomaviruses and cancer: from basic studies to clinical application. *Nat. Rev. Cancer* **2**, 342–350 (2002).

4. Tang, K.-W., Alaei-Mahabadi, B., Samuelsson, T., Lindh, M. & Larsson, E. The landscape of viral expression and host gene fusion and adaptation in human cancer. *Nat. Commun.* **4**, 2513 (2013).

5. Cantalupo, P. G., Katz, J. P. & Pipas, J. M. Viral sequences in human cancer. *Virology* **513**, 208–216 (2018).

6. Walboomers, J. M. M. *et al.* Human papillomavirus is a necessary cause of invasive cervical cancer worldwide. *J. Pathol.* **189**, 12–19 (1999).

7. Schwarz, E. *et al.* Structure and transcription of human papillomavirus sequences in cervical carcinoma cells. *Nature* **314**, 111–114 (1985).

8. Perz, J. F., Armstrong, G. L., Farrington, L. A., Hutin, Y. J. F. & Bell, B. P. The contributions of hepatitis B virus and hepatitis C virus infections to cirrhosis and primary liver cancer worldwide. *J. Hepatol.* **45**, 529–538 (2006).

9. Shafritz, D. A., Shouval, D., Sherman, H. I., Hadziyannis, S. J. & Kew, M. C. Integration of Hepatitis B Virus DNA into the Genome of Liver Cells in Chronic Liver Disease and

Hepatocellular Carcinoma. *N. Engl. J. Med.* **305**, 1067–1073 (1981).

10. Uemura, N. *et al. Helicobacter pylori* Infection and the Development of Gastric Cancer. *N. Engl. J. Med.* **345**, 784–789 (2001).

11. Watanabe, T., Tada, M., Nagai, H., Sasaki, S. & Nakao, M. Helicobacter pylori infection induces gastric cancer in mongolian gerbils. *Gastroenterology* **115**, 642–8 (1998).

12. zur Hausen, H. The search for infectious causes of human cancers: Where and why. *Virology* **392**, 1–10 (2009).

13. Goodwin, S., McPherson, J. D. & McCombie, W. R. Coming of age: ten years of next-generation sequencing technologies. *Nat. Rev. Genet.* **17**, 333–351 (2016).

14. Niedobitek, G. *et al.* Detection of human papillomavirus type 16 DNA in carcinomas of the palatine tonsil. *J. Clin. Pathol.* **43**, 918–21 (1990).

15. Gillison, M. L. *et al.* Evidence for a Causal Association Between Human Papillomavirus and a Subset of Head and Neck Cancers. *J. Natl. Cancer Inst.* **92**, 709–720 (2000).

16. Castellarin, M. *et al.* Fusobacterium nucleatum infection is prevalent in human colorectal carcinoma. *Genome Res.* **22**, 299–306 (2012).

17. Kostic, A. D. *et al.* Genomic analysis identifies association of Fusobacterium with colorectal carcinoma. *Genome Res.* **22**, 292–8 (2012).

18. Repass, J. *et al.* Replication Study: Fusobacterium nucleatum infection is prevalent in human colorectal carcinoma. *Elife* **7**, (2018).

19. Hanahan, D. & Weinberg, R. A. Hallmarks of cancer: the next generation. *Cell* **144**, 646–74 (2011).

20. Riley, D. R. *et al.* Bacteria-Human Somatic Cell Lateral Gene Transfer Is Enriched in Cancer Samples. *PLoS Comput. Biol.* **9**, e1003107 (2013).

21. Zapatka, M. *et al.* The landscape of viral associations in human cancers. *bioRxiv* 465757 (2018). doi:10.1101/465757

22. Khoury, J. D. *et al.* Landscape of DNA virus associations across human malignant cancers: analysis of 3,775 cases using RNA-Seq. *J. Virol.* **87**, 8916–26 (2013).

23. International Cancer Genome Consortium, T. I. C. G. *et al.* International network of cancer genome projects. *Nature* **464**, 993–8 (2010).

24. Gibbs, R. A. *et al.* A global reference for human genetic variation. *Nature* **526**, 68–74 (2015).

25. Wood, D. E. & Salzberg, S. L. Kraken: ultrafast metagenomic sequence classification using exact alignments. *Genome Biol.* **15**, R46 (2014).

26. Hu, Z. *et al.* Genome-wide profiling of HPV integration in cervical cancer identifies clustered genomic hot spots and a potential microhomology-mediated integration mechanism. *Nat. Genet.* **47**, 158–163 (2015).

27. Young, L., Sung, J., Stacey, G. & Masters, J. R. Detection of Mycoplasma in cell cultures. *Nat. Protoc.* **5**, 929–934 (2010).

28. Li, H. & Durbin, R. Fast and accurate long-read alignment with Burrows-Wheeler transform. *Bioinformatics* **26**, 589–95 (2010).

29. Caygill, C. P., Hill, M. J., Braddick, M. & Sharp, J. C. Cancer mortality in chronic typhoid and paratyphoid carriers. *Lancet (London, England)* **343**, 83–4 (1994).

30. Scanu, T. *et al.* Salmonella Manipulation of Host Signaling Pathways Provokes Cellular Transformation Associated with Gallbladder Carcinoma. *Cell Host Microbe* **17**, 763–774 (2015).

31. Geller, L. T. *et al.* Potential role of intratumor bacteria in mediating tumor resistance to the chemotherapeutic drug gemcitabine. *Science (80-.).* **357**, 1156–1160 (2017).

32. Feng, Y. *et al.* Metagenomic and metatranscriptomic analysis of human prostate microbiota from patients with prostate cancer. *BMC Genomics* **20**, 146 (2019).

33. Kripalani-Joshi, S. & Law, H. Y. Identification of integrated epstein-barr virus in nasopharyngeal carcinoma using pulse field gel electrophoresis. *Int. J. Cancer* **56**, 187–192 (1994).

34. Morton, C. *et al.* Mapping of the human Blym-1 transforming gene activated in Burkitt lymphomas to chromosome 1. *Science (80-.).* **223**, 173–175 (1984).

35. Robinson, K. M., Crabtree, J., Mattick, J. S. A., Anderson, K. E. & Dunning Hotopp, J. C. Distinguishing potential bacteria-tumor associations from contamination in a secondary data analysis of public cancer genome sequence data. *Microbiome* **5**, 9 (2017).

36. Thompson, K. J. *et al.* A comprehensive analysis of breast cancer microbiota and host gene expression. *PLoS One* **12**, e0188873 (2017).

37. Mazzoni, E. *et al.* Significant Association Between Human Osteosarcoma and Simian Virus 40. doi:10.1002/cncr.29137

38. Ramanan, P., Deziel, P. J. & Wengenack, N. L. Gordonia bacteremia. *J. Clin. Microbiol.*

51, 3443–7 (2013).

39. Ding, X. *et al.* Bacteremia due to Gordonia polyisoprenivorans: case report and review of literature. *BMC Infect. Dis.* **17**, 419 (2017).

40. Gupta, M., Prasad, D., Khara, H. S. & Alcid, D. A rubber-degrading organism growing from a human body. *Int. J. Infect. Dis.* **14**, e75–e76 (2010).

41. Austen, B. *et al.* Mutations in the ATM gene lead to impaired overall and treatment-free survival that is independent of IGVH mutation status in patients with B-CLL. (2005). doi:10.1182/blood-2004-11-4516

42. Balthazar, E. J., Megibow, A. J. & Hulnick, D. H. Cytomegalovirus esophagitis and gastritis in AIDS. *AJR. Am. J. Roentgenol.* **144**, 1201–4 (1985).

43. Lepiller, Q., Tripathy, M. K., Di Martino, V., Kantelip, B. & Herbein, G. Increased HCMV seroprevalence in patients with hepatocellular carcinoma. *Virol. J.* **8**, 485 (2011).

44. Leonardsson, H., Hreinsson, J. P., Löve, A. & Björnsson, E. S. Hepatitis due to Epstein–Barr virus and cytomegalovirus: clinical features and outcomes. *Scand. J. Gastroenterol.* **52**, 893–897 (2017).

45. Bruix, J. & Llovet, J. M. Hepatitis B virus and hepatocellular carcinoma. *J. Hepatol.* **39**, 59–63 (2003).

46. Lai, C.-C. *et al.* Infections caused by unusual Methylobacterium species. *J. Clin. Microbiol.* **49**, 3329–31 (2011).

47. Langevin, S., Vincelette, J., Bekal, S. & Gaudreau, C. First case of invasive human infection caused by Cupriavidus metallidurans. *J. Clin. Microbiol.* **49**, 744–5 (2011).

48. Ugge, H. *et al.* Acne in late adolescence and risk of prostate cancer. *Int. J. cancer* **142**, 1580–1585 (2018).

49. Davidsson, S. *et al.* Frequency and typing of Propionibacterium acnes in prostate tissue obtained from men with and without prostate cancer. *Infect. Agent. Cancer* **11**, 26 (2016).

50. COHEN, R. J., SHANNON, B. A., McNEAL, J. E., SHANNON, T. & GARRETT, K. L. *PROPIONIBACTERIUM ACNES* ASSOCIATED WITH INFLAMMATION IN RADICAL PROSTATECTOMY SPECIMENS: A POSSIBLE LINK TO CANCER EVOLUTION? *J. Urol.* **173**, 1969–1974 (2005).

51. Mahlen, S. D. Serratia infections: from military experiments to current practice. *Clin. Microbiol. Rev.* **24**, 755–91 (2011).

52. Fessler, J., Matson, V. & Gajewski, T. F. Exploring the emerging role of the microbiome in cancer immunotherapy. *J. Immunother. Cancer* **7**, 108 (2019).

53. Motzer, R. J. *et al.* Nivolumab versus Everolimus in Advanced Renal-Cell Carcinoma. *N. Engl. J. Med.* **373**, 1803–13 (2015).

54. Sung, W.-K. *et al.* Genome-wide survey of recurrent HBV integration in hepatocellular carcinoma. *Nat. Genet. Vol.* **44**, (2012).

55. Welcome | ICGC Data Portal. Available at: https://dcc.icgc.org/. (Accessed: 6th June 2019)

56. Index von /vol1/ftp/. Available at: ftp://ftp.1000genomes.ebi.ac.uk/vol1/ftp/. (Accessed: 6th June 2019)

57. European Nucleotide Archive < EMBL-EBI. Available at: https://www.ebi.ac.uk/ena. (Accessed: 6th June 2019)

58. Afgan, E. *et al.* The Galaxy platform for accessible, reproducible and collaborative biomedical analyses: 2018 update. *Nucleic Acids Res.* **46**, W537–W544 (2018).

59. Li, H. *et al.* The Sequence Alignment/Map format and SAMtools. *Bioinformatics* **25**, 2078–2079 (2009).

60. Picard Tools - By Broad Institute. Available at: http://broadinstitute.github.io/picard/. (Accessed: 6th June 2019)

61. Quinlan, A. R. & Hall, I. M. BEDTools: a flexible suite of utilities for comparing genomic features. *Bioinformatics* **26**, 841–842 (2010).

62. Bolger, A. M., Lohse, M. & Usadel, B. Trimmomatic: a flexible trimmer for Illumina sequence data. *Bioinformatics* **30**, 2114–20 (2014).

63. Blankenberg, D. *et al.* Manipulation of FASTQ data with Galaxy. *Bioinformatics* **26**, 1783–5 (2010).

64. Rognes, T., Flouri, T., Nichols, B., Quince, C. & Mahé, F. VSEARCH: a versatile open source tool for metagenomics. *PeerJ* **4**, e2584 (2016).

65. The R Foundation for Statistical Computing R version 3.3.2. (https://www.r-project.org/).

66. Escapa, I. F. *et al.* New Insights into Human Nostril Microbiome from the Expanded Human Oral Microbiome Database (eHOMD): a Resource for the Microbiome of the Human Aerodigestive Tract. *mSystems* **3**, e00187-18 (2018).

67. Dewhirst, F. E. *et al.* The Human Oral Microbiome. *J. Bacteriol.* **192**, 5002–5017 (2010).

68. HOMD :: Human Oral Microbiome Database. Available at: http://www.homd.org/index.php?name=HOMD. (Accessed: 6th June 2019)

69. de Goffau, M. C. *et al.* Recognizing the reagent microbiome. *Nat. Microbiol.* **3**, 851–853 (2018).

70. Salter, S. J. *et al.* Reagent and laboratory contamination can critically impact sequence-based microbiome analyses. *BMC Biol.* **12**, 87 (2014).

71. Jervis-Bardy, J. *et al.* Deriving accurate microbiota profiles from human samples with low bacterial content through post-sequencing processing of Illumina MiSeq data. *Microbiome* **3**, 19 (2015).

72. Leon, L. J. *et al.* Enrichment of Clinically Relevant Organisms in Spontaneous Preterm-Delivered Placentas and Reagent Contamination across All Clinical Groups in a Large Pregnancy Cohort in the United Kingdom. *Appl. Environ. Microbiol.* **84**, e00483-18 (2018).

73. Laurence, M., Hatzis, C. & Brash, D. E. Common Contaminants in Next-Generation Sequencing That Hinder Discovery of Low-Abundance Microbes. *PLoS One* **9**, e97876 (2014).

74. Glassing, A., Dowd, S. E., Galandiuk, S., Davis, B. & Chiodini, R. J. Inherent bacterial DNA contamination of extraction and sequencing reagents may affect interpretation of microbiota in low bacterial biomass samples. *Gut Pathog.* **8**, 24 (2016).

75. Camacho, C. *et al.* BLAST+: architecture and applications. *BMC Bioinformatics* **10**, 421 (2009).

76. Wally, N. *et al.* Plasmid DNA contaminant in molecular reagents. *Sci. Rep.* **9**, 1652 (2019).

77. Embedding projector - visualization of high-dimensional data. Available at: https://projector.tensorflow.org/. (Accessed: 6th June 2019)

78. Morpheus. Available at: https://software.broadinstitute.org/morpheus/. (Accessed: 6th June 2019)

79. Li, H. & Durbin, R. Fast and accurate short read alignment with Burrows-Wheeler transform. *Bioinformatics* **25**, 1754–1760 (2009).

80. Wick, R. R., Judd, L. M., Gorrie, C. L. & Holt, K. E. Unicycler: Resolving bacterial genome assemblies from short and long sequencing reads. *PLOS Comput. Biol.* **13**, e1005595 (2017).

81. Sondka, Z. *et al.* The COSMIC Cancer Gene Census: describing genetic dysfunction across all human cancers. *Nat. Rev. Cancer* **18**, 696–705 (2018).

82. Warden, C. D., Yuan, Y.-C. & Wu, X. *Optimal Calculation of RNA-Seq Fold-Change Values*. *International Journal of Computational Bioinformatics and In Silico Modeling* **2**, (2013).

83. Warden, C. D., Kanaya, N., Chen, S. & Yuan, Y.-C. BD-Func: a streamlined algorithm for predicting activation and inhibition of pathways. *PeerJ* **1**, e159 (2013).

84. Ashburner, M. *et al.* Gene ontology: tool for the unification of biology. The Gene

Ontology Consortium. *Nat. Genet.* **25**, 25–9 (2000).